EAGLE LAKE CLIMATE CHANGE DURING THE HOLOCENE AND DURING THE LAST 100 YEARS

A THESIS

Presented to the Department of Geological Sciences

California State University, Long Beach

In Partial Fulfillment

of the Requirements for the Degree

Master of Science in Geology

Committee Members:

Lora Stevens-Landon, Ph.D. (Chair)
Benjamin Hagedorn, Ph.D.
Nathan Onderdonk, Ph.D.

College Designee:

Richard J. Behl, Ph.D.

By Mounga E. Nonu

B.S., 2012, University of California, Riverside

December 2017

ABSTRACT

EAGLE LAKE CLIMATE CHANGE DURING THE HOLOCENE AND DURING THE LAST 100 YEARS

By

Mounga E Nonu

December 2017

Multi-proxy comparative analyses of sediment from Eagle Lake, including total organic carbon (TOC), δ13C and δ15N composition of bulk organic material, n-alkane distribution, and biogenic silica, was used to document hydroclimatic changes during the early and late Holocene. Eagle Lake is currently located near the transition zone of the North American Precipitation Dipole, with the timing of precipitation showing a winter-wet scenario common to the Pacific Northwest, but overall precipitation (e.g., aridity) showing a Pacific Southwest pattern. The width and position of this transition is poorly constrained during the Holocene and is hypothesized to have migrated, particularly in response to the North American Monsoon. Eagle Lake is thus ideal in providing insights to the past positions of the dipole. Multi-proxy analyses result in differences between the early and late Holocene at Eagle Lake. TOC is lower in the early Holocene, however C:N ratios are much more variable indicating a transition from algal source material to terrestrial and back to algal material prior to the Mazama ash. There are also greater fluctuations of biogenic silica during the early Holocene, suggesting rapid changes in productivity.

To place these Holocene changes within the context of known climatic and anthropogenic conditions of the 20th century, a ~100 year record of hydrologic change is compared to droughtand lake-level drops induced by the formation of the Bly Tunnel. Importantly, the effects

of the tunnel on lake level is superimposed on the 1930s drought, making it difficult to disentangle the two impacts. However, the TOC and C:N ratios clearly mirror variations in lake level suggesting that they are effective indicators of Holocene variations.

ACKNOWLEDGEMENTS

This thesis would not be completed if not for the amazing support, advice and guidance from family and friends.

To Dr. Lora Stevens, without you, none of this would be possible. Thank you for being an amazing advisor, mentor, and "academic mom." Thank you for igniting my love for Eagle Lake and helping me understand how incredibly complex, but beautiful lake mud can really be. Your unwavering support, motivation and drive is sincerely appreciated. Thank you for allowing me to grow as a research scientist and for every opportunity you've given me. I will forever be grateful to you. I would like to thank my committee members, Dr. Benjamin Hagedorn and Dr. Nate Onderdonk, for their help. Their feedback and guidance with my research and writing was essential in the completion of my thesis.

I would also like to thank Dr. Varenka Lorenzi, for not only keeping me employed, but for her help in understanding the organic chemistry component of my thesis.

Thank you to all my friends for your support, help, and beer: James Minor, Earl O'Bannon, AJ White, Kelsey Dorion, Brendan Neel, Lindsey Jeans-Shaw and Rosemarie Wrigley.

Thank you to my brotherhood, the boys of TeleTae'Fiu, for a relaxing remedy around the bowl after a hectic school/work week.

Thank you Mom and Dad for your constant support and for pushing me to be better. Thank you to all my family and siblings, Melesisi, Gladys, Michael, and Mosi for always helping when I need it. Last, but not least, Thank you Lute for always supporting me and pushing me to be a better person academically and in life.

Saame 23: veesi 1 – Ko Hoku Tauhi a Siohova, e ikai Teu Masiva

TABLE OF CONTENTS

LIST OF TABLES

LIST OF FIGURES

CHAPTER 1

INTRODUCTION

In the western United States, many cities are dependent on melting mountain snowpack to replenish reservoirs, rivers and groundwater that provide water for human consumption and agriculture. Rapid changes in climate, particularly severe droughts, can drastically decrease the available water in reservoirs (Cook et al., 2015). A record-breaking drought (Figure 1) started in California in 2012 and spread across the western United States by the end of 2013. By 2014, state-level "drought emergencies" were declared in California, Oregon and Washington (Swain et al., 2014). The drought continued until winter of 2017 due to the "ridiculously resilient ridge" (Swain, 2015). California's drought period of extremely low precipitation and high temperatures was attributed to several causes including the persistent northward deflection of the cool-season storm track by a recurring anomalous anticyclone ("ridiculously resilient ridge") over the far northeastern Pacific (Swain et al., 2016). There were concomitant increases in temperature as well, which further impacted the moisture balance. What caused this ridge of high pressure to persist for five years is debated, with global warming considered a possible trigger (Swain, 2015).

Anthropogenic climate change may have been a contributing factor to this severe drought, but even in the absence of anthropogenic effects, the western United States is a region with high interannual and interdecadal climate variability. The multiple processes responsible for precipitation variability create large uncertainty concerning future precipitation (Choi et al., 2016; Langenbrunner et al., 2015; Wise, 2016). Paleoclimate data help frame current events through a broader view of possible manifestations of the climate system. Evidence illustrating past climate can be used to assess the accuracy of model simulations of past climate conditions that then help

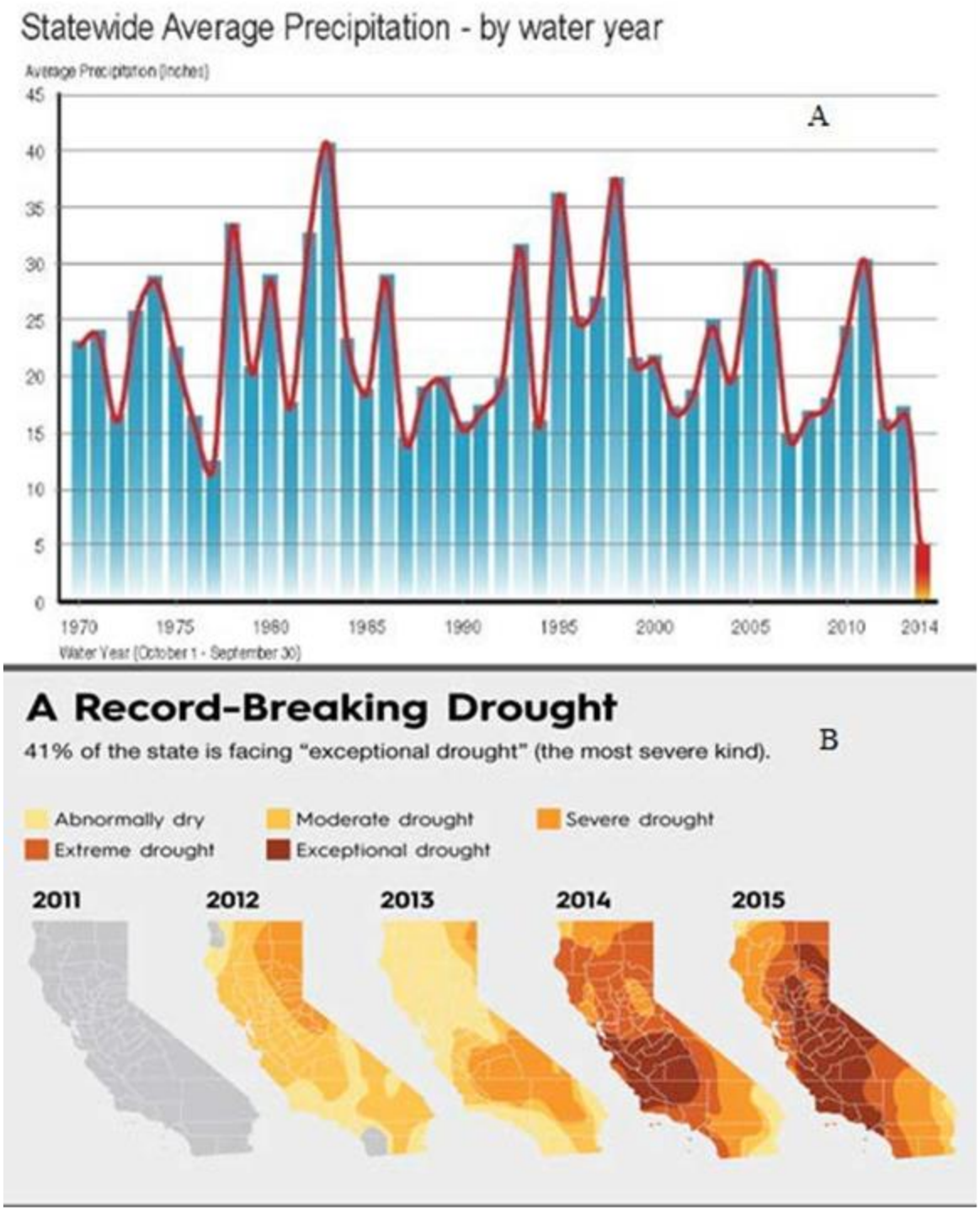

FIGURE 1. Top) Statewide average precipitation from 1970-2014. Notice 2014 drastic decrease in precipitation compared to the past (source: U.S. Dept. of Water). Bottom) Visual representation of changes in drought severity from 2011 to 2015 (source: U.S. Dept. of Agriculture, NOAA).

to constrain future projections (Cook et al., 2007; Thompson et al., 2011).

Lakes serve as archives for regional climate change, and their sedimentary sequences are well suited for multi-proxy paleoclimate studies. Combining records from multiple lake sites can lead to a better understanding of the spatial extent and severity of specific climate processes and the interactions among different climate sub-systems over time. Lake records that are most suitable for paleoclimate research are those resulting from the gradual and steady accumulation of biogenic sediments (Felmy and Weare, 1986; Li and Ku, 1997; Steinment et al., 2010). Small lakes with minimal riverine or tectonic influence are usually more sensitive to variations in precipitation, temperature and nutrient balance. Unfortunately, the constant, undisturbed accumulation of such records can be complicated, obscured, or even destroyed by human activity (e.g., mining activities or land development), tectonic instability and desiccation. In such settings where these factors pose risks, utmost attention should be paid in order to clearly understand the depositional environment prior to data collection.

This study focuses on the climate record archived in Eagle Lake, Lassen County, northeastern California (Figure 2). Eagle Lake is unique in both its potential climatic record and the opportunity to observe how human and tectonic interferences can be imprinted on the sedimentary record.

Site Description

Eagle Lake (40.6540°N, 120.7439°W) is a large freshwater lake located on the eastern flank of the Sierra Nevada Mountains in northern California, ~26 km north of Susanville and ~62 km east of Mount Lassen. The lake is located on the southern margin of the Modoc Plateau, a large volcanic province of Miocene-Quaternary age, with flat-lying basaltic lava flows that extend northward into Oregon (White and Crider, 2006). The present size and configuration

FIGURE 2. Site map of Eagle Lake in California. Map includes locations of Pine Creek, Lassen Peak, Susanville, CA, Eagle Lake Watershed (ELW) and the Bly Tunnel. Inset is a photo of Bly Tunnel outlet 1924 (picture from Lola L. Tanner; base map from National Geographic Society).

of Eagle Lake formed when Tertiary lava flows blocked drainage into the Willow Creek Valley, thus creating a basin behind the damned lava flow (Gester, 1962). The southern and central basin is surrounded by Pliocene hornblende-pyroxene andesite of Merrill Mountain, andesitic lava flows of Antelope Mountain and Pleistocene basalt of the Brockman Flat. The northern basin is surrounded by Tertiary-aged basalts and andesitic flows (Grose et al., 1992) (Figure 3).

Eagle Lake has no natural surface outlet and is considered a hydraulically closed basin. A seasonal inlet, Pine Creek, is fed by spring runoff from snow pack and is the major source of inflow. Intermittent flows from two minor streams, Papoose and Merrill Creeks, contribute water during spring. Additional input into the lake occurs year-around via underground springs (Bateson, O., pers. comm., 2016). Water leaves Eagle Lake through evaporation, ground water flow, and seepage into the abandoned Bly tunnel. The Bly Tunnel was built in the 1920s to transfer water to neighboring valleys for agricultural use but was sealed in the 1970s (Purdy, 1988) and re-sealed again in 2012.

Eagle Lake is divided into three basins (Figure 3). The southern basin is the deepest with (Z_{max} = ~18 m). The central basin and Troxel Bay are to the north and both have Zmax = ~2 m. Eagle Lake is dimictic with spring and fall overturns. However, the southern basin is the only basin that stratifies thermally during summer with a resultant oxygen-poor hypolimnion (Maslin and Boles, 1978). Water quality data collected in October 2011 (Stevens, pers. comm., 2017) indicate that the southern basin was well mixed with isothermal conditions, and relatively uniform values of pH, dissolved oxygen and salinity (Figure 4a). At Stone's Landing in Troxel Bay, the water column was also well mixed, but showed a temperature inversion at the bottom. This inversion also resulted in lower dissolved oxygen content (Figure 4b). The temperature inversion might indicate an introduction of ground water at that location.

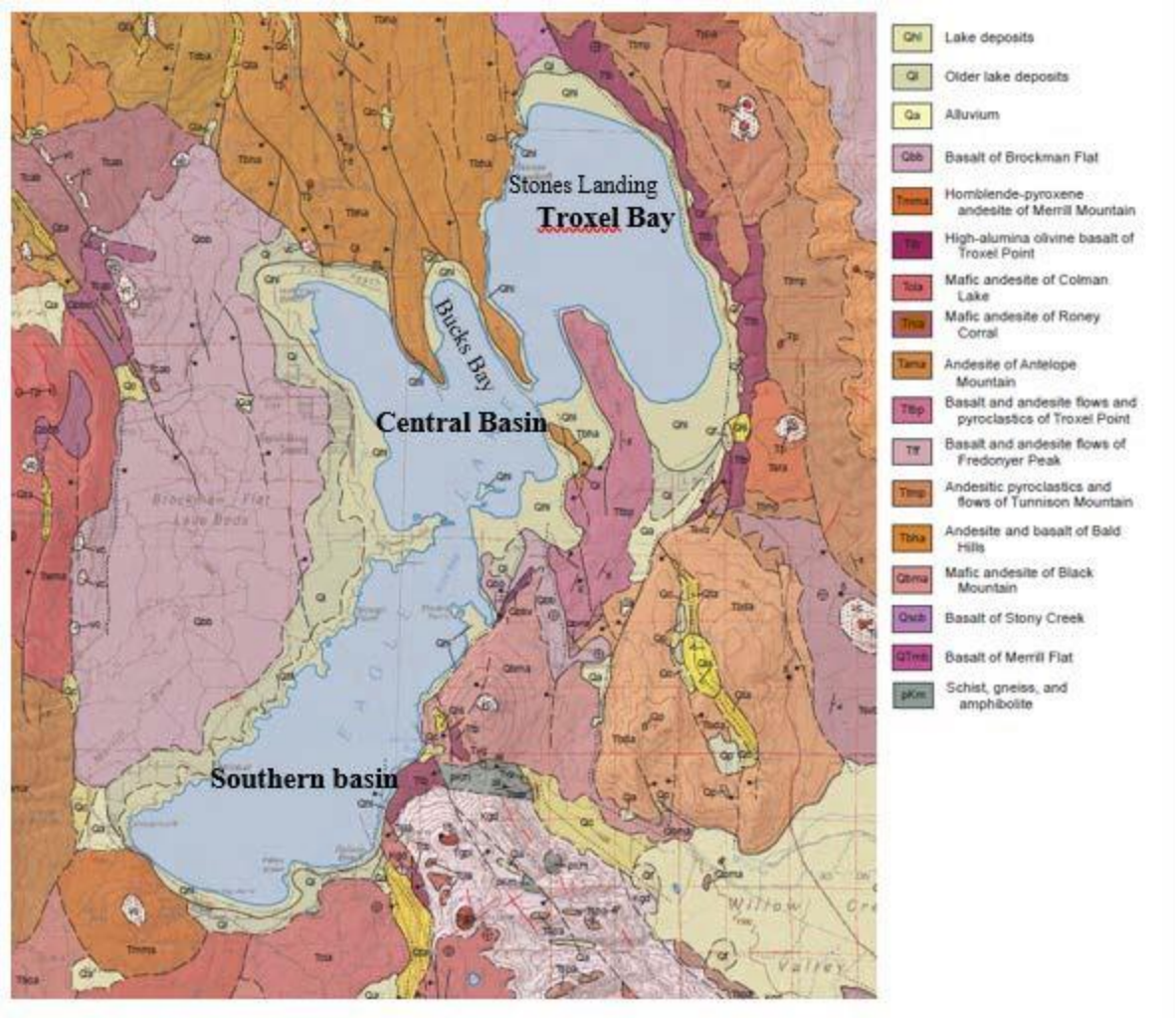

FIGURE 3. Condensed geologic map of the Eagle Lake 30' x 60' quadrangle, CA. Approximate stratigraphic relationships highlighted around Eagle Lake. Light yellow colors are late Pleistocene-Holocene aged, dark purple and orange colors are Pliocene aged, and dark green is Mesozoic age (from Grose et al., 1992).

Discussions with local residents indicate that ice can be thinner or non-existent in certain places in Troxel Bay, adding support for the idea of a ground water discharge zone in this basin.

Older water quality data from 1974 indicate that the lake had a pH of 8.95 and alkalinity of 410 mg/L as CaCO3 (Cahoon, 1974). Tributary surface waters have low concentrations of dissolved solids, chlorides, nitrates, and sulfates and, unlike Eagle Lake water, the tributaries have a low alkalinity (~37 mg/L), which highlights the evaporative concentration in this closed basin. The average weighted nutrient concentration for Eagle Lake water is 0.29 ppm nitrogen and 0.04 ppm phosphorus (Cahoon, 1974). Ground water data sampled from irrigation wells along the south, west and north shores have similar values to Eagle Lake water (0.25 ppm N and ~0.07 ppm P) (Cahoon, 1974). Houses on the shores of both Troxel Bay and the central basin may contribute high suspended loads of phosphorous and iron through their septic systems. Furthermore, both basins are shallow and thus likely oxygenated by wind-driven mixing, which could re-suspend nutrients from decaying organic matter. Thus, the nutrient loading is expected to be higher in the northern basins.

Regional Climate Setting

The general climate of northern California is temperate with dry, warm summers. It falls under the Köppen-Geiger classification, 'Csb' (main climate: warm temperate, precipitation: summer dry, temperature: warm summer) (Kottek et al., 2006). During summer months, northern California is dominated by subtropical high pressure cells, with dry sinking air making rainfall unlikely. In the winter months, the polar jet stream and associated periodic storms reach into northern California bringing rainfall and snow. The winter wet regime is true of California, which receives almost all of its precipitation during the winter, fall and spring seasons. The majority of California has relatively mild winters (~13°C) and very warm summers (~22°C);

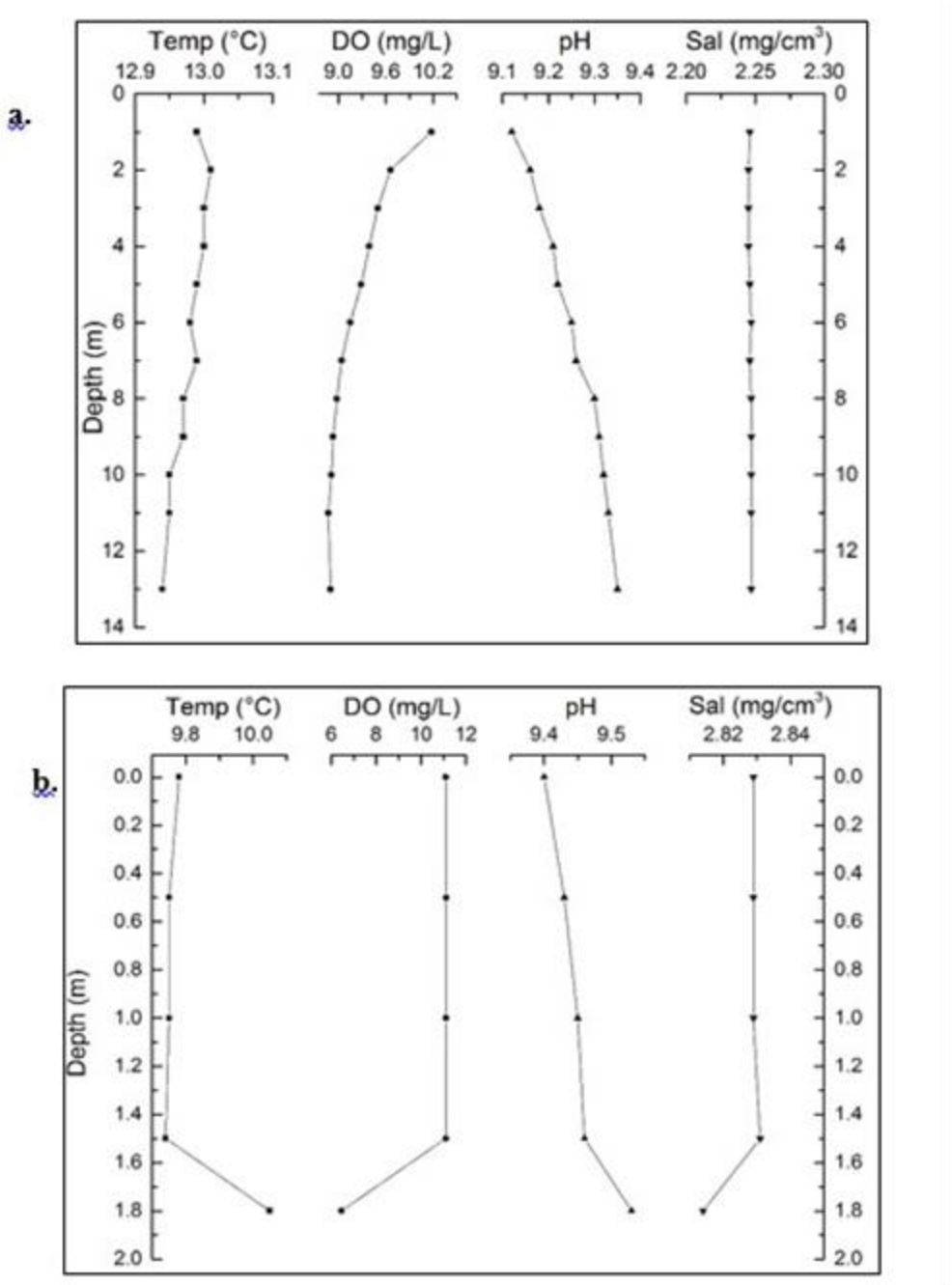

FIGURE 4. Water quality of the Eagle Lake southern basin (4a). Water quality at Stone's Landing in Troxel Bay (4b).

however, winter and summer temperatures can vary greatly.

Because of Eagle Lake's position on the leeward side of the Sierra Nevada Mountains, precipitation and temperature are greatly affected by the Sierra Nevada rain shadow. Monthly climate data from the Susanville Municipal Airport (approximately 26 km south of Eagle Lake) cover the period, 1900 – 2013 (Figure 5). Mean monthly temperature ranges from -5.5 ℃ to 25.1 ℃ with a yearly average of 9.7 ℃. The annual precipitation averages 3.04 cm, although long-term annual precipitation data indicate that the wettest months are during the late fall and winter (i.e., October – March) with the spring and summer months (April – September) contributing only about 40% of the total annual precipitation. The influence of the terrain causes Eagle Lake climate to behave similarly to that of a desert climate year-round, little to no rain and months of extreme heat waves.

The North American Precipitation Dipole

The western United States is characterized by two modern climatic regimes: the wet Pacific Northwest (PNW) and the dry Pacific Southwest (PSW) (Figure 6). The PNW and PSW tend to vary inversely with one another, resulting in contrasting precipitation patterns, western streamflow variability, and overall climate variability. The general climate of the PNW is characterized by high precipitation over a prolonged period of time. The PSW climate is considered dry with hot, dry summers and mild winters with little to no rainfall. This inverse behavior is known as the North American Precipitation Dipole (NAPD) (Figure 6). This dipole is obvious during synoptic hydroclimatic oscillations, such as the El Niño-Southern Oscillation (ENSO) and Pacific Decadal Oscillation (PDO) (McCabe et al., 2004; Redmond and Koch, 1991).

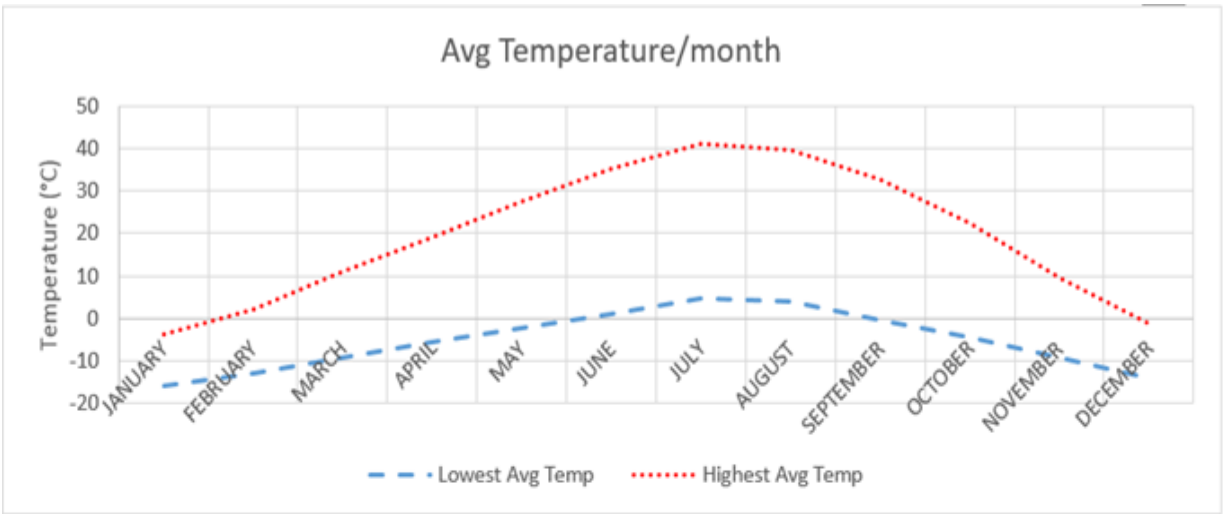

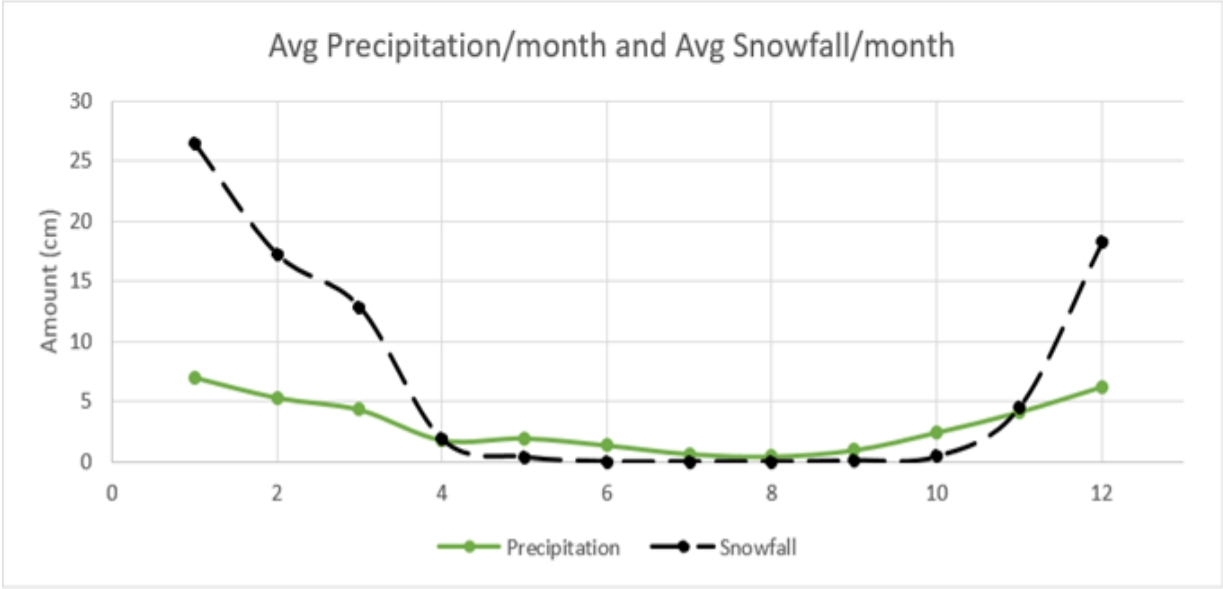

FIGURE 5. 1900-2013 monthly climate data. Temperature (dash vs dash-dotted line), total precipitation (solid line) and snowfall averages (long dash) at Susanville Municipal Airport located 26 miles south of Eagle Lake (source: NOAA).

Modern Synoptic Climate Variability

The present hydroclimatic state of the western United States is strongly influenced by synoptic atmospheric features, including the Aleutian Low (Barron and Anderson, 2011; Dettinger et al., 1998; McCabe et al., 2004), that affect the amount of available moisture. These features vary at spatial and temporal scales. One dominant synoptic pattern is El Niño-Southern Oscillation (ENSO), which dominates interannual climate variability observed globally (Ropelewski and Halpert, 1987, 1989). As a climate phenomenon, ENSO has the ability to change the global atmospheric circulation, which in turn, influences temperature and precipitation along the western United States. ENSO occurs in two opposite phases, "El Niño" and "La Niña" (Figure 7). El Niño is considered to have above-average sea surface temperatures (SST) in the central and eastern tropical Pacific Ocean. The Easterlies are weakened and precipitation increases over the central Pacific Ocean and decreases over Indonesia. La Niña is cooling of the ocean surface in central and eastern Pacific Ocean with increased precipitation over Indonesia, decreased precipitation over the central Pacific Ocean and stronger Easterlies.

El Niño and La Niña affect the western US differently. During an El Niño phase, trade winds are weakened bringing warm surface waters to the western US. Warmer SSTs fuel and intensify a southward shift of the jet stream and storm tracks, flooding much of southwest US and causing the northwest US to become dryer than usual. In contrast, La Niña usually brings an unusual intensification of trade winds moving warmer Pacific waters westward causing an upwelling of cooler waters in the eastern Pacific. The jet stream is displaced northward causing the PSW to experience drought-like conditions with cooler temperatures and heavy rains in the PNW (Piechota et al., 1997; Ropelewski and Halpert, 1987; McCabe and Dettinger, 1999).

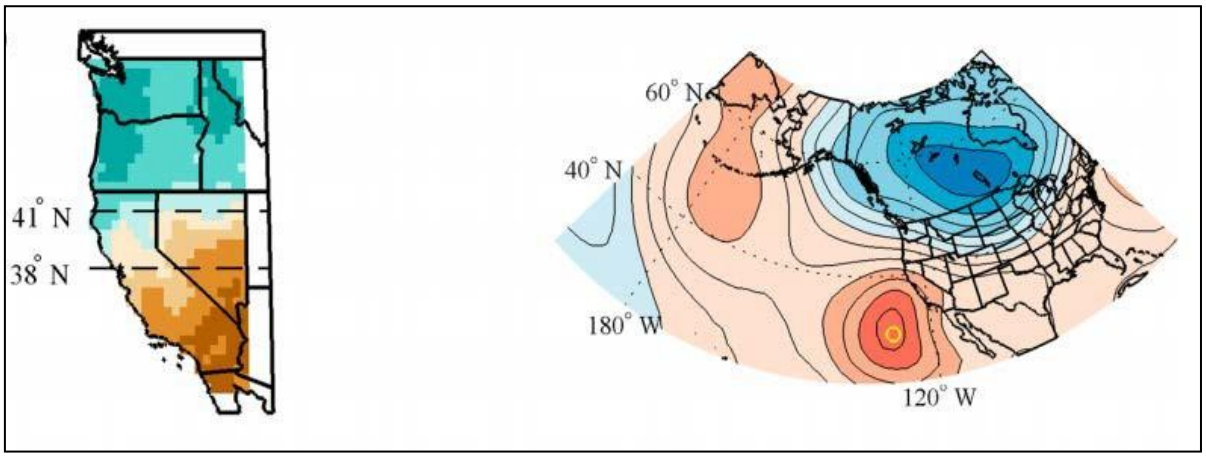

FIGURE 6. Left picture is a reconstructed standard precipitation index (from Mckee et al., 1993) of the western US. Blue indicates positive and wet units of the PNW and brown indicates negative dry units of the PSW. White band indicates the transition zone of the NAPD. On the right is the geopotential anomalies for north-wet (blue)/south-dry (red) years, 1500 – 2010 C.E. (from Wise, 2016).

Another dominant pattern in the modern climate system of the western US is the Pacific Decadal Oscillation (PDO) (Figure 8) (Mantua and Hare, 2002), which influences water supplies, snow pack, and drought conditions at multi-decadal (~20-40 year) frequencies over much of the region (McCabe et al., 2004). The PDO is an El Niño-like pattern, but persists for much longer time periods and is most visible in the North Pacific/North American Sector (Mantua et al., 1997; Zhang et al., 1996). The PDO also has warm/positive phases and cold/negative phases. During a positive phase, the western North Pacific cools and the waters in the region of the North American west coast warm. The result is increased winter precipitation in the southwestern US and along the southeastern Alaskan coast, whereas a region of decreased winter precipitation occurs in the northwestern US and southwestern Canada. These SST patterns and precipitation anomalies are largely reversed during a negative PDO phase. The atmospheric link between the SSTs and precipitation is the strength and position of the Aleutian Low (AL). The AL is stronger and shifts to the east during a positive PDO and weakened and pushed to the west during a negative PDO (Cayan et al., 1999). Interactions of the PDO and Atlantic Multidecadal Oscillation (AMO) create complex patterns of drought over the entire US (McCabe et al., 2004). The AMO is an index of detrended SST anomalies averaged over the North Atlantic from 0-70° N and has been identified as an important mode of climate variability (McCabe et al., 2004). Evaluation of the spatial variability of observed and simulated drought frequency over specific periods (e.g., the 1930s drought and the Northeastern droughts of the 1950s and 1960s) (Figure 9) reveals that the spatial distribution of drought frequency can be binned into four general scenarios (McCabe and Dettinger, 1999). A positive AMO and positive PDO (Figure 9C) produce a spatial drought similar to the 1930s drought. With positive AMO and negative PDO,

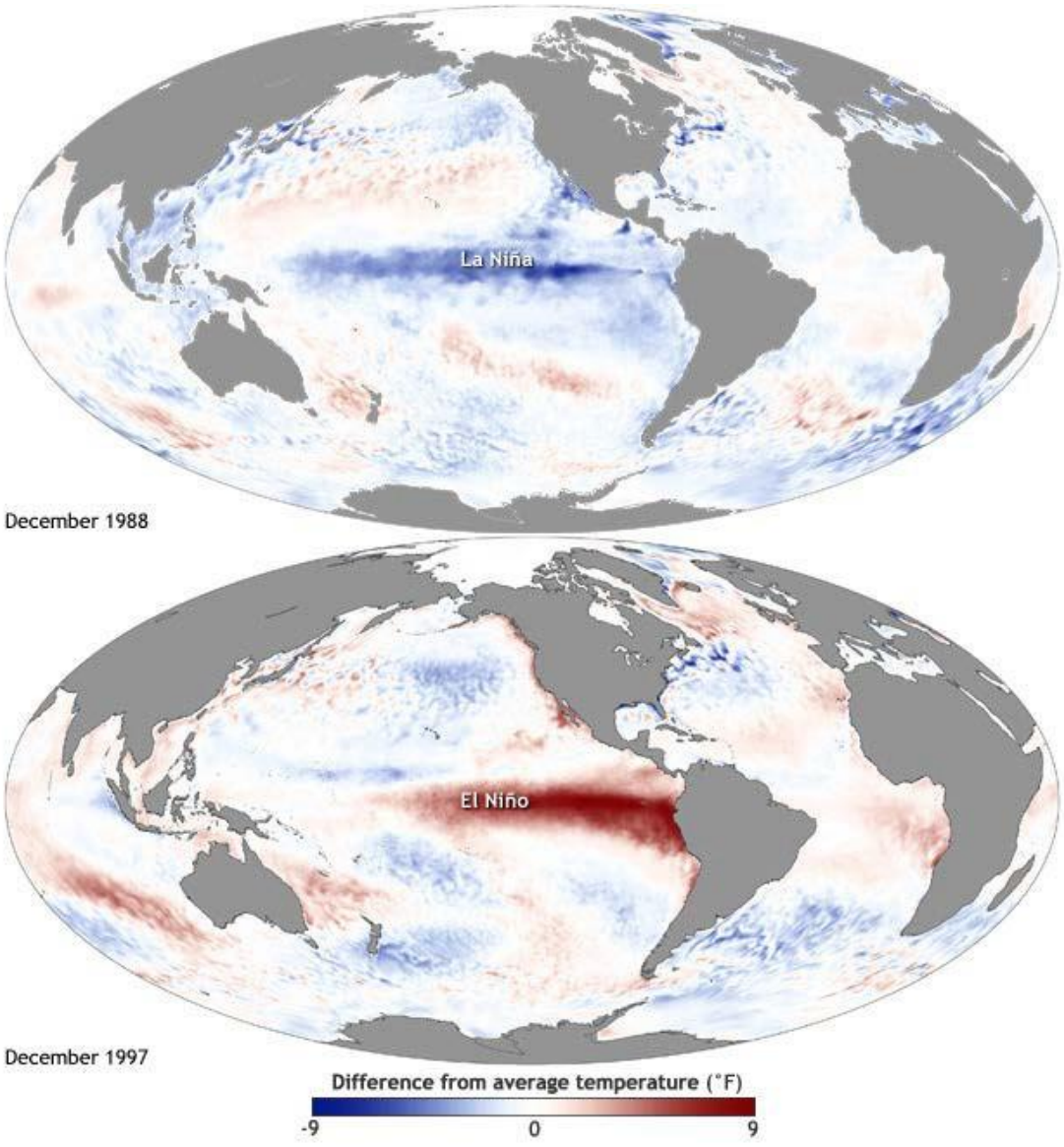

FIGURE 7. ENSO as a coupled climate phenomenon. Maps of sea surface temperature anomalies in the Pacific Ocean during a strong La Niña (top, Dec. 1988) and El Niño (bottom, Dec 1997) (Source: NOAA; Climate.gov).

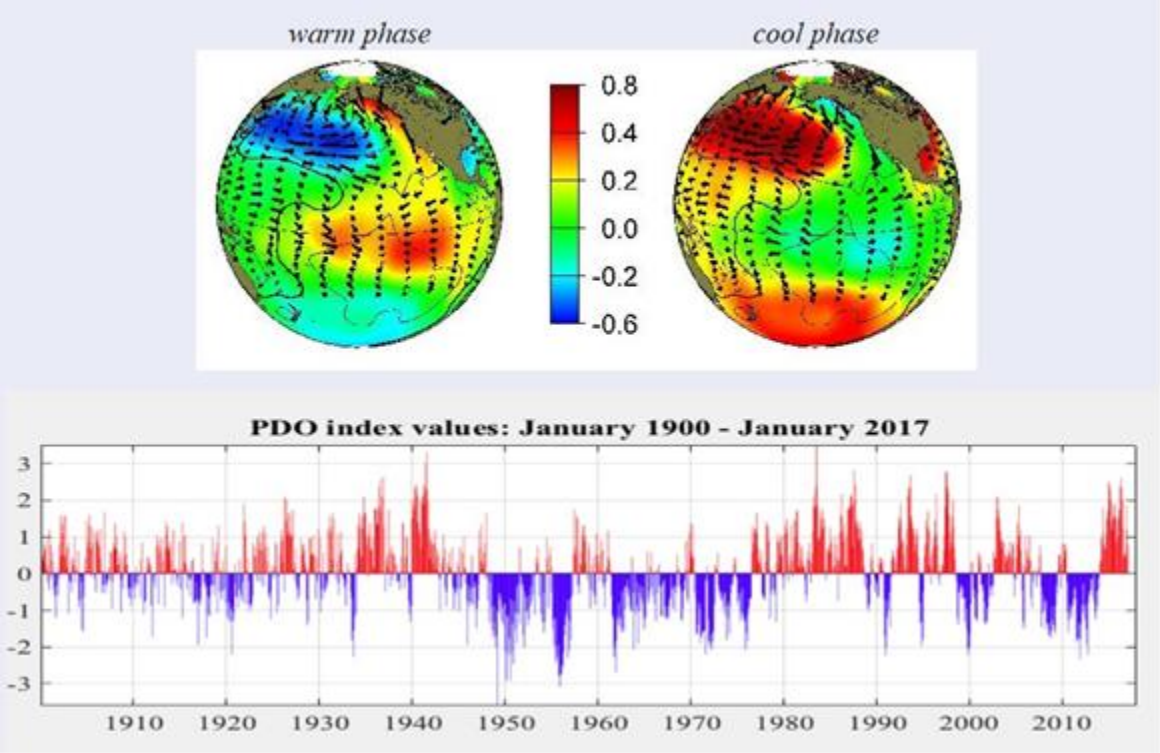

FIGURE 8. The Pacific Decadal Oscillation is a long-lived El Niño-like pattern of Pacific climate variability. Comparison of typical warm and cold PDO/El-Niño sea surface temperatures (colors), sea level pressure (contours) and wind anomalies (arrows) (from JISAO top graphic). Graphic comparing monthly PDO values from 1900 – 2017 (from Zhang et al., 1996).

the pattern is similar to the 1950s drought (Figure 9D). However, the pattern of the recent 5-year drought does not resemble any of these scenarios.

Sediment Proxies of Hydroclimatic Change

Sedimentary proxies are indirect measures of past climatic changes. In order to constrain interpretations, multiple proxies were measured in the sediment of Eagle Lake. All proxies used in this thesis indicate some level of lake productivity, which can be indirectly related to lake level and thus moisture balance.

Percent total organic carbon (TOC) is often a coarse first assessment of any lake study. However, interpretation of TOC does not yield unique conclusions as this proxy reflects the balance between algal productivity and organic matter preservation. High amounts of TOC usually indicate high levels of productivity. Increased productivity is often correlated to increased precipitation via direct input of precipitation and precipitation runoff (Galloway and Cowling, 1978). However, high amounts of TOC can also result from enhanced organic matter increased precipitation via direct input of precipitation and precipitation runoff (Galloway and Cowling, 1978). However, high amounts of TOC can also result from enhanced organic matter preservation due to low oxygen (El Frihmat et al., 2015). It can be extremely difficult to disentangle these two factors, especially since the first (high productivity) often results in the second (low oxygen levels).

Atomic and/or molar ratios of total organic carbon to total nitrogen (C:N) in lake sediments is often used as an indicator of the relative amounts of terrestrial and algal sources in sediment organic source matter (Meyers, 1994, 1997; Meyers and Ishiwatari, 1993; Prahl et al., 1980; Sweeney and Kaplan, 1980). Algal matter has atomic C:N ratios between 4 and 10, and emergent macrophytes/terrestrial matter have C:N ratios greater than 20. High C:N ratios are

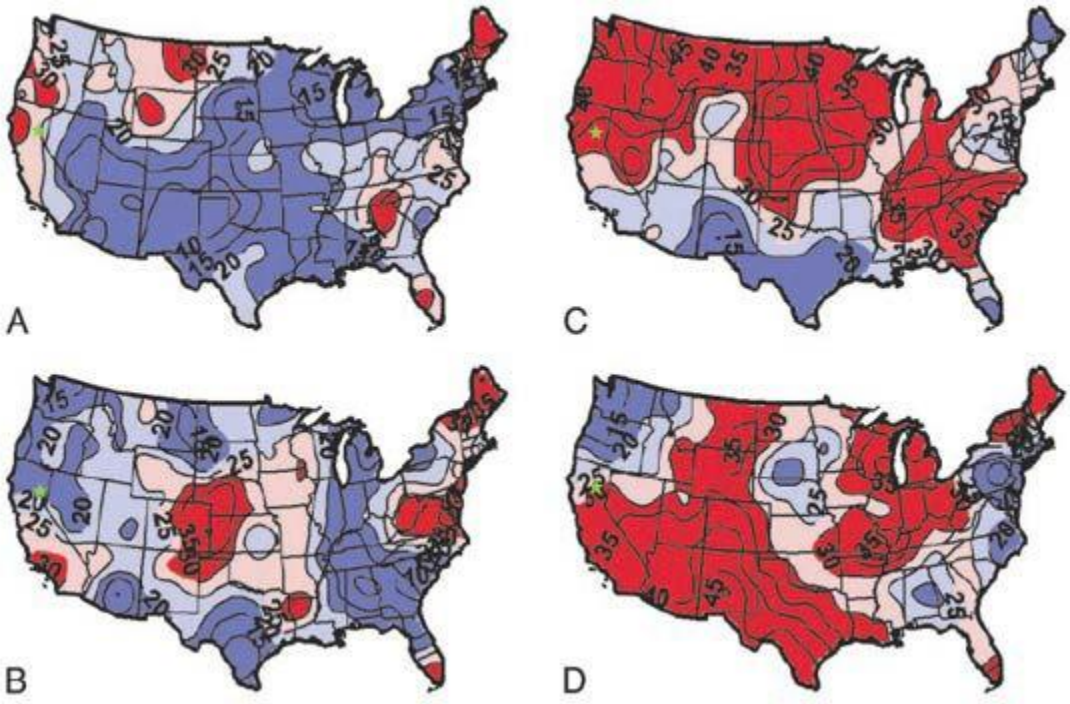

FIGURE 9. Drought frequency (in percent of years) for positive and negative regimes of the PDO and AMO. (A) positive PDO, negative AMO (1977 – 1994) (B) negative PDO, negative AMO (1964-1976) (C) positive PDO, positive PDO (1923 – 1943) (D) negative PDO, positive AMO (1944 – 1963) (from McCabe et al., 2004). Eagle Lake indicated by green star.

often associated with lowered lake levels in conjunction with drought. Shallow waters in response to lower lake levels and drought are ideal for emergent macrophytes, which result in higher C:N values. However, it is also interpreted that high C:N ratios can indicate a higher influx of terrestrial organic matter from streams during wetter periods. Alternatively, during wetter conditions, an influx of nutrients from streams may increase algal productivity and thus lower C:N ratios. These data are never interpreted alone due to conflicting possibilities.

Normal-alkanes are straight-chained saturated hydrocarbons with no functional groups. Both terrestrial plants and algae typically produce a range of alkanes with a strong odd-over-even-dominance and one or two dominant chain lengths (Eglington and Logan, 1991). Algae typically synthesize n-alkanes with short chain lengths and have n-C15, n-C17, or n-C19 as the dominant compounds. Terrestrial vascular plants are dominated by long-chained n-alkanes in the range of C23 to C35 with a dominance of C27, C29, and C31. By analyzing the n-alkane distribution and quantifying relationship between algae and terrestrial plants through a $P_{aqueous}$ ratio (Ficken et al., 2000), a signature between terrestrial, emergent macrophytes, and algae matter can be determined.

Percent biogenic silica (wt. % BSi) provides an estimate of both diatom abundance and thus diatom productivity (Conley and Schelske, 2001). These siliceous microfossils are commonly used in paleolimnological studies related to eutrophication and acidification of surface waters. The measure of wt. % BSi is a more robust proxy for productivity than %TOC, however the same caveat of preservation applies. Biogenic opal can be dissolved in high pH waters, which could be a concern in Eagle Lake.

Ostracodes are micro-crustaceans found in both marine and terrestrial environments. They are either benthic, living in sediment surface or subsurface, or live on emergent

macrophytes. Ostracodes have an outer shell (carapace) made of two halves. They molt up to nine times and precipitate their shells from ions taken directly from the water, which means that the ostracode calcite reflects the host chemistry (Caporaletti, 2011). Because the shells are secreted over a short amount of time, their shell chemistry represents the chemistry of the host water at a specific time (Holmes, 1996; Chivas et al., 1986). Samples from Troxel and Bucks Bay were isolated and informally identified, but no geochemical analysis was conducted due to the paucity of the ostracodes and shortness of the record. However, the presence of ostracodes only in the northern basins suggest that they may be an indicator of warmer, shallower water.

Study Objectives

This thesis includes two distinct studies at Eagle Lake that use the same proxies, but which have different research foci. The studies are encompassed in separate chapters; however, because they use the same proxies, the methods are presented in a separate chapter to avoid redundancy.

The first study (Chapter 3) attempts to discern shifts in the North American Precipitation Dipole between the early (~7.5 to 10.8 ka BP) and late Holocene (~1-2 ka BP) using lake productivity and sediment structure as proxies of lake level and moisture availability. The early and late Holocene are selected for comparison due to their different climatic boundary conditions. The early Holocene had higher seasonality (e.g., high summer insolation and low winter insolation) and was still experiencing the influence of the waning ice sheets. The late Holocene more closely resembles modern solar and ice configurations.

The second study (Chapter 4) is a detailed look at the 20th century lake conditions that were strongly influenced by both climatic (e.g., the 1930s drought) and anthropogenic impacts (e.g., the construction of the Bly Tunnel). The 20th century climate is often used to validate the

changes seen in the sedimentary record. But if human activities overprint the climate signal, are these validation studies useful? That is, can human-induced reductions in lake level be separated from drought-induced reductions? If so, are there unique fingerprints? From the human construction of the Bly Tunnel in 1925, to the natural drought of the 1930s, this thesis will try to determine how these disturbances affected lake productivity.

CHAPTER 2

METHODS

Core Collection

Two Livingston piston cores (Wright, 1967) were collected in October 2011 and March 2016 from the southern basin and Bucks Bay, respectively. The core from the southern basin (ELSB11) was collected in ~20 m water depth (Figure 10) and consists of seven non-overlapping, contiguous 1-m drives. Cores are often collected from the deepest basin of the lake as these represent the most uninterrupted sequences of sedimentation. A failed drive during the coring resulted in an unknown loss of sediment in the middle Holocene.

Overlapping drives were taken from Bucks Bay in 2.6 m water depth (Figure 10). The Bucks Bay core (ELBB16) consists of 1.5 m of contiguous sediment. Cores from this shallow bay were collected to document the lake level changes accompanying the 1930s drought, which would not be well represented in the deeper basin.

Core Sampling

Samples, 5 mm in thickness, were collected in the upper and lower sections of the core ELSB11 to represent the late (~0 – 2 ka BP) Holocene and early (~8 – 10 ka BP) Holocene, respectively. These sections were initially subsampled at 5 cm intervals. Subsampling intervals increased for areas of interest, such as banded layers and diatomaceous laminations. ELBB16 was subsampled at 5 cm intervals with samples being 5 mm in thickness.

Dating

Two macrofossils from 81.5 and 375 cm depth in ELSB-11 were dated by AMS radiocarbon at the W.M. Keck Carbon Cycle Accelerator Mass Spectrometry Laboratory at UC

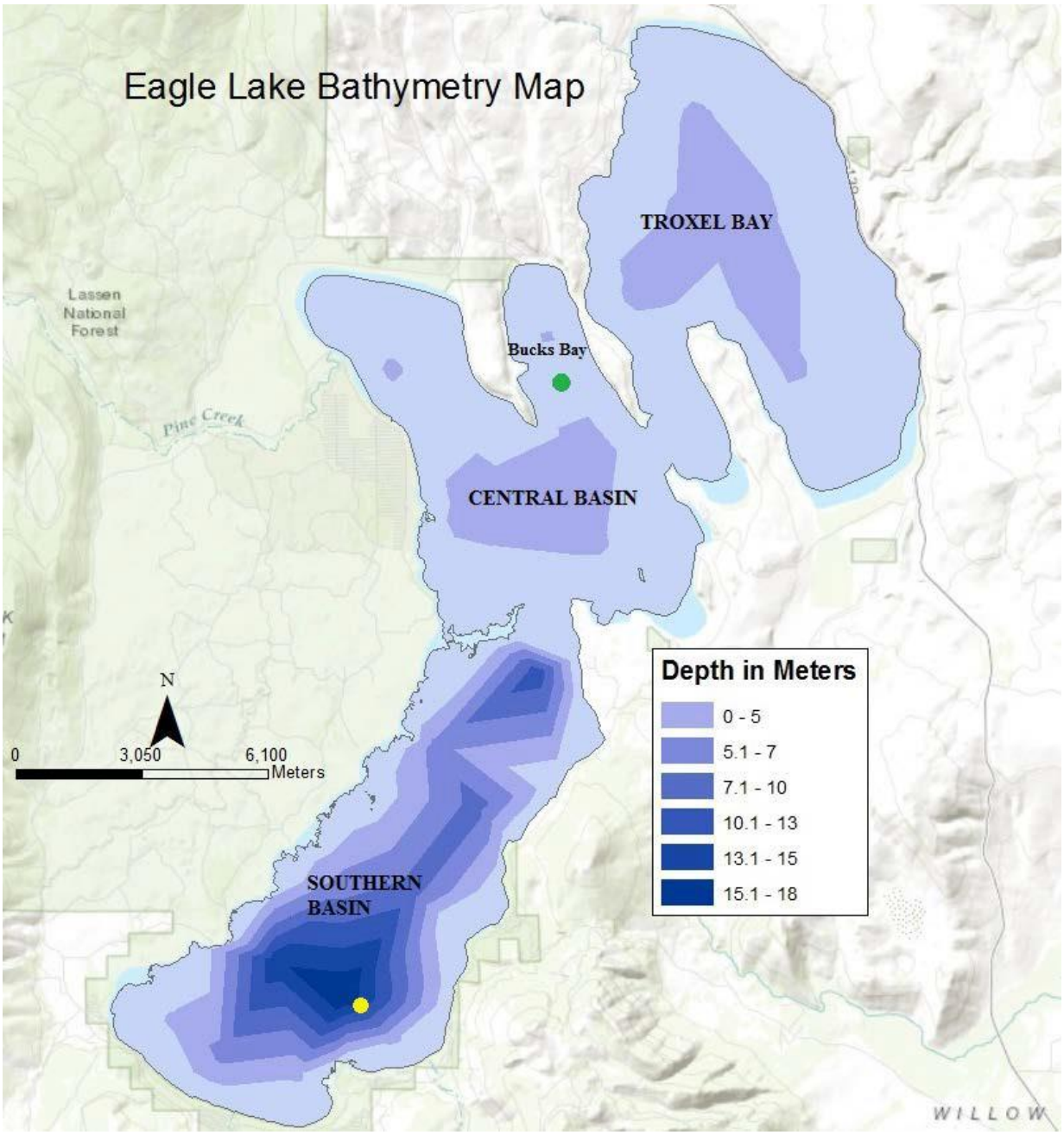

FIGURE 10. Eagle Lake bathymetry map. Yellow circle in southern basin is the ELSB11 core and green circle in Bucks Bay is the ELBB16 core (base map from ESRI, DeLorne, and USGS).

Irvine. The radiocarbon dates were calibrated with Calib 7.1 (Stuiver and Reimer, 1993) and reported as cal ka BP.

Total Organic Carbon and Total Inorganic Carbon

Total carbon (TC) and total inorganic carbon (TIC) were analyzed on a UICTM CM5014 CO2 Coulometer. Total organic carbon (TOC) was calculated from the difference of these two. The coulometer is a titration method to determine carbon content of sediments and other materials. The coulometer is coupled to either a furnace or an acidification module, which produce CO2 gas through combustion of carbon-bearing material at 950°C or acidification of carbonates, respectively. For TC, freeze-dried samples were homogenized and weighed into ceramic boats and introduced to the furnace component. The liberated CO2 gas was then carried into the coulometer cell and converted to µg carbon/minute. For TIC, freeze-dried sediment was weighed into Teflon boats and acidified with ten percent perchloric acid. A single standard, pure calcite, was used to check that all C was liberated and measured. Pure calcite should produce ~12% TC or TIC. The acceptable error is 12 ± 0.4%. TOC and TIC values are reported as % C (Appendix A)

Carbon:Nitrogen Ratios

Weight percent carbon and nitrogen ratios were analyzed using a Costech ECS 4010 CHNSO elemental analyzer. Small aliquots of samples were placed in centrifuge tubes and reacted overnight with 5 – 10 ml of 0.5 M hydrochloric acid to remove any inorganic carbon. Samples were centrifuged, repeatedly rinsed with high purity deionized water then freeze-dried. Dried samples were homogenized and weighed into silver capsules, which were then placed in tin capsules and folded into small spheres. Each run included several bypasses and blanks. Thecalibration curve was calculated from Acetanilide and quality assurance was checked with

Standard Reference Material 1944 New York/New Jersey Waterway Sediment. C:N analysis included the standard Acetanilide at four levels, bypasses and blanks. Data are reported as wt. %C, wt. %N, and the C:N values calculated from the ratio of the first two (Appendix B).

Normal-Alkane Distribution

Freeze-dried and homogenized sediment samples, 1-2 g in mass, were extracted by soxhlet with dichloromethane (DCM) at ~35℃ for 24 hours. Samples were combined with 5 g of sodium sulfate and placed in cellulose thimbles that were pretreated with DCM for over 24 hours. The thimbles had to be treated with DCM because the plant-based cellulose of the thimble resulted in high background levels of n-alkanes. The hydrocarbon fractions in the extracts were separated by silica-gel and alumina column chromatography. The hydrocarbon fraction was slowly percolated through the column, and the column was flushed with DCM. The extracts are concentrated through a rotary evaporator and then percolated through the column again, but flushed with hexane and concentrated again. 49451-U C7 – C30 Saturated Alkanes certified reference material was used as a retention index marker probe. Analysis included blanks, blanks spiked with the standard, and recovery surrogates. The final extract was pipetted into 1 milliliter vials and analyzed on an Agilent 5975 Inert MSD Gas Chromatography-Mass Spectrometer (GC/MS). IIRMES lab coordinator, Dr. Varenka Lorenzi quantified the data, which are reported in μg/g (Appendix C).

Biogenic Silica

Biogenic silica was measured following the wet-alkaline method of Conley and Schelske (2001). Thirty mg of freeze-dried and homogenized sediment samples were weighed into 250 25 polycarbonate Boston Round bottles. Forty ml of 1% sodium carbonate was added, and samples were then leached at 70 ℃ for a period of 4 hours. One ml aliquots of solution were

withdrawn at 1-, 2-, 3- and 4-hour intervals. Soluble Si is based on the formation of a blue silicomolybdate color complex. Liquid extracts were treated with ammonium molybdate, which produced heteropoly acids. Addition of oxalic acid eliminated excess phosphates, and ascorbic acid was used to reduce silicomolybdate complex to a stable heteropoly blue complex (Conley and Schelske, 2001). The amount of silicomolybdate is reflected in the intensity of the blue color measured by the absorbance of 660 nanometer wavelength light on a Cary™ UV-Vis spectrophotometer. Absorbance was converted to concentration via a 7-point calibration curve from stock solutions (10, 20, 40, 60, 100, 150, 200 mg/L). Due to slight variations in the actual amount of sediment used, the concentration was converted to wt. % silica using the following formula,

$$\%BSi = \left(\frac{\frac{weight\ of\ Si\ Extracted}{25}}{30mg}\right) * 100 \qquad Eq.\ 1$$

Data are reported as wt. % biogenic silica (Appendix D).

Ostracodes

Sediment samples were wet-sieved at 63 μm. Material caught in the sieve was placed on a filter and dried in the oven. The ostracodes were picked with a fine-tipped brush and separated by species. Each species can be an indication of water conditions during its time of life. The adult carapaces were cleaned with HPLC grade ethanol and preliminary scanning electron microscopy was done for two distinct ostracode species.

CHAPTER 3

EARLY HOLOCENE – LATE HOLOCENE CLIMATE COMPARISON

Tracking the North American Precipitation Dipole in the Holocene at Eagle Lake

Comparison of climates during the early and late Holocene allow us to examine the effects of different climatic boundary conditions on moisture availability in the western United States. For example, greater summer insolation and less winter insolation resulted in maximum seasonality in the early Holocene, expressed as warmer summers and colder winters relative to today (Barron and Anderson, 2011; Bird and Kirby, 2006). During the early Holocene (~10 ka – 7.5 ka) the summer insolation maximum strengthened the North American Monsoon (Dean, 1974; Enzel et al., 1992; Kutzbach, 1981), which in turn resulted in high effective moisture in the PSW (Barron et al., 2012; Bird and Kirby, 2006; Enzel et al., 1992; Thompson et al., 2011). Simultaneously, the climate of the PNW was influenced by the atmospheric effects of the waning Laurentide and Cordilleran ice sheets and the moderation of temperature by the ice (Shuman et al., 2002; Wright, 1972). The colder temperatures over the ice resulted in atmospheric subsidence that produced a high-pressure system and easterlies across the northern US (COHMAP, 1988). This had the added effect of displacing the westerlies further to the south (e.g., across the PSW). As the ice sheet retreated, the high-pressure system moved northward and westerlies prevailed as they do today.

Early Holocene proxy records from sites across the PNW confirm that climate conditions were likely warmer and drier than today. For example, plant communities included species that thrive in dry climates, such as Artemisia (Whitlock and Bartlein 1993; Grigg and Whitlock, 1998). Pollen data show that these shrub-dominant communities extended as far north as British Columbia and Alberta, indicating a 40 percent reduction in moisture relative to today (Chatters,

1991; Mehringer, 1985). Isotopic records from shells also indicate warmer and drier conditions in the region (Davis and Muehlenbachs, 2001).

In general, the solar and ice configurations of the late Holocene result in climate similar to what we see today. The major exception is the Little Ice Age (~1300 – 1870) (Mann, 2002), which resulted from reduced sun spot activity (Mauquoy et al., 2002) and caused an expansion of mountain glaciers (Maurer et al., 2012) in the western US. The late Holocene is characterized by generally wet conditions in the PNW and dry conditions in the PSW. The study at Lower Bear Lake in southern California (PSW) confirms these dry conditions via high total carbon and C:N ratios (Kirby et al., 2012). Kirby et al. (2012) also documented mega-scale droughts in Lake Elsinore (PSW).

Alternatively, the PNW experienced the opposite overall climate. The late Holocene vegetation is consistent with cooler wetter summers compared with the early Holocene. Changes in vegetation assemblages during the late Holocene, such as an increase of Abies species and P.menziesii in northern forests, indicate high effective moisture (Briles et al., 2011) possibly resulting from a weakening of the northeastern Pacific subtropical high-pressure system (Briles et al., 2011).

Multiple lake sites confirm the general position of the NAPD. Holocene reconstructions of stream flow and lake level change have been developed for Lake Elsinore (974 km south of Eagle Lake) and Lower Bear Lake, California (Kirby et al., 2007, 2010) in the PSW. During the early Holocene, Lake Elsinore and Lower Bear Lake were generally wet. Tulare Lake (450 km south of Eagle Lake), central California, was dry during the late Holocene and wet during the early Holocene (Negrini et al., 2006). Environmental conditions were constructed in the central California coast dating back 3300 years (Cowart and Byrne, 2013). The authors concluded that

during the late Holocene, the central coast was dry, placing it in the PSW. Similarly Zaca Lake (598 km south of Eagle Lake) was dry during the late Holocene, and thus in the PSW (Mensing, 1998). In contrast, Pyramid Lake (120 k southeast of Eagle Lake) was wet during the early Holocene, also placing it in the PSW zone. Briles et al. (2005) concluded that Bolan Lake (419 km northwest of Eagle Lake) was warm and dry climate during the early Holocene and thus falls within the PNW region. Based on these comparisons, it is apparent that the North American Precipitation Dipole (NAPD) has existed throughout the Holocene and can be broadly mapped by these locations.

However, the boundary between the PNW and PSW, alternating climate regimes of the NAPD is not sharp or fixed in space and time. Today, the boundary is located at approximately 40°N latitude (Dettinger et al., 1998), but throughout the Holocene, it is believed to have migrated north or south depending on the mean climate state as controlled by the boundary conditions (e.g., insolation, ice sheets). Since the winter season precipitation in the Western US is the dominant source of water supply for several states, the relationship between synoptic climate changes and the NAPD has allowed forecasts within the PNW and PSW (Barron and Anderson, 2011; Benson et al., 2002; Mensing et al., 2004). However, the area within the transition zone does not have this predictive capability as the zone may fall in either regime. Understanding the spatial distribution of the boundary, as well the changes within the zone, requires a basic understanding of modern synoptic climate. Today, Eagle Lake is located today within the NAPD transition zone and thus may be used to examine whether the NAPD boundary was displaced northward during the early Holocene as suggested by Anderson (2011).

Results

Core Lithology

Sediment from the early Holocene in Eagle Lake core, ELSB11, looks different than the late Holocene. The early Holocene section comprises four drives: ELSB11-D10 (I), ELSB11-D9 (H), ELSB11-D8 (G) and ELSB11-D7 (F) and the late Holocene section comprises two drives: ELSB11-D2 (B) and ELSB11-D1 (A) (Figure 10). True depths are 290 – 590 cm and 0 – 130 cm for the early and late Holocene, respectively. It should be noted that 0 cm does not represent the sediment-water interface as there is approximately 30 cm of core that is too loose and soupy to be captured by the piston corer.

The early Holocene section is dominated by layers with distinct diatomaceous laminations and banding, whereas the late Holocene section has no laminations, uniform dark brown gyttja with the exception of a distinct, red-brown layer (Figure 11). The entire core is made of compacted organic-rich sediment, known as gyttja, deposited at the bottom of lakes. A stratigraphic profile is shown in (Figure 12) and the Munsell color designations in Table 1.

Age Model

Uncalibrated and calibrated radiocarbon ages are reported in Table 2. A chronological model is not possible given the loss of sediment in the failed drive. However, the dates confirm the overall age of the late Holocene and early Holocene sediment packets. Using the single radiocarbon date and the age of the Mazama ash, the average sedimentation rate during the early Holocene (375 – 575 cm) is 0.8 mm/yr. A late Holocene sedimentation rate is not possible due to the single date at 215 cm.

Total Organic and Inorganic Carbon

All samples measured had only a miniscule amount of %TIC, thus only the %TOC is reported. There is a clear distinction between the early and late Holocene periods. The early Holocene section ranges between 5 and 10 %TOC, and the late Holocene section ranges between

TABLE 1. Munsell Color Scheme for ELSB11

Core	Depth (cm)	Munsell Color	Color Notation	
ELSB11-LH	0 - 28	Dusky brown	5 YR 2/2	
	29 - 36	Dark grayish brown	5 YR 3/2	
	36 - 40	Light olive gray	5Y 5/2	
	41 - 48	red-brown	10R 5/4	
	49 - 130	Dark yellowish brown	10YR 4/2	
ELSB11-EH	295 - 305	Dusky brown	5YR 2/2	
	305 - 313	Medium light gray	7 N7	(Mazama Ash)
	314 - 317	Pale yellowish brown	10 YR 6/2	
	317 - 347	Dark yellowish brown	10 YR 4/2	
	347 - 392	Dusky brown	5 YR 2/2	
	392 - 400	Dark yellowish brown	10 YR 4/2	
	401 - 408	Dusky brown	5 YR 2/2	
	408 - 412	Olive brown color	5 Y 4/4	
	413- 470	Dark yellowish brown	10 YR 4/2	
	471 - 520	dusky yellow brown	5 YR 4/2	(Diatomaceous Laminations)
	521 - 590	Dark yellowish brown	10 YR 4/2	

TABLE 2. Radiocarbon Dates for ELSB11

Depth (cm)	Lab ID	Sample ID	^{14}C Year BP	Median Age (cal yr. BP)
215	UCIAMS-103154	ELSB-D2-21.5 cm	2915 ± 15	3004 - 3074
575	UCIAMS-103155	ELSB-D10-70 cm	8970 ± 340	9391 - 11096
375	N/A	Mazama ash	*7627 ± 150	7627

*Date is Mazama ash from Bacon (1983).

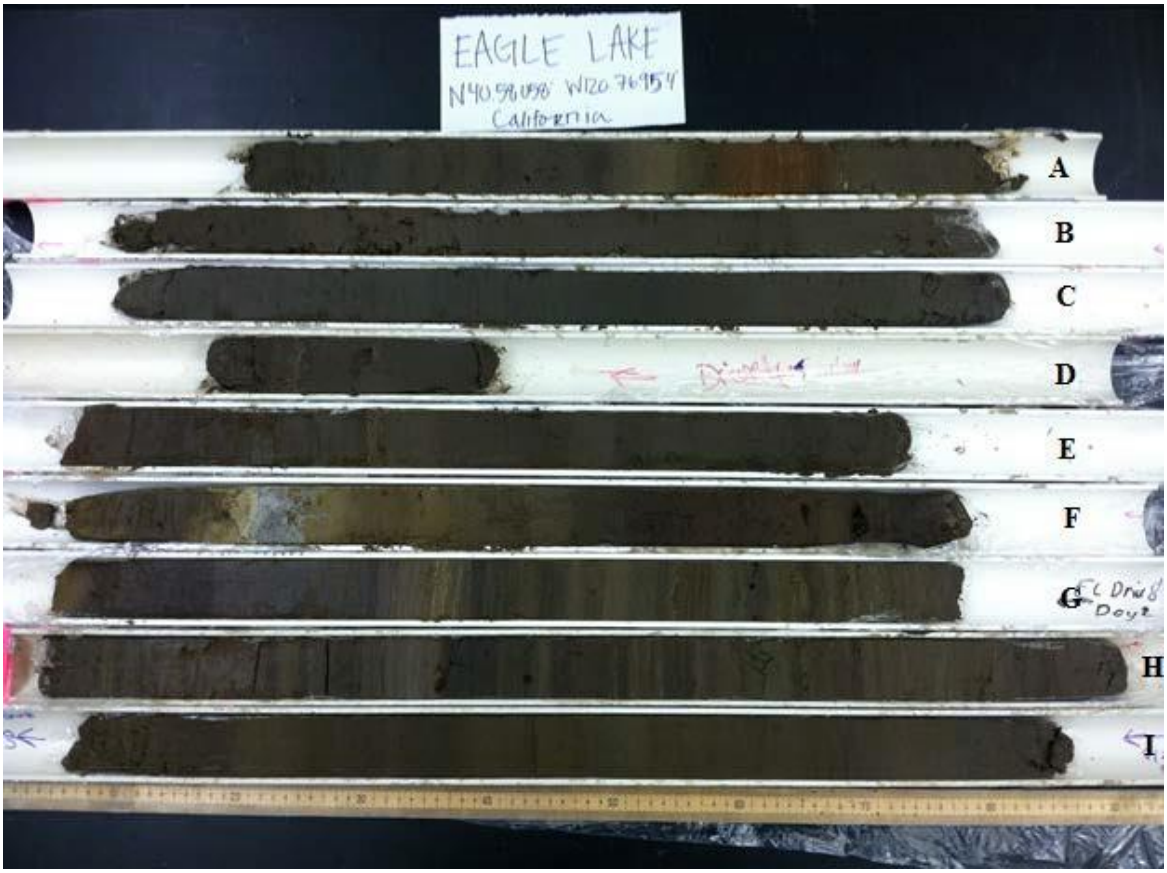

FIGURE 11. Photograph of ELSB11. Drive A is the youngest and I is the oldest. Stratigraphic up is to the left for each drive. Multi-proxy analyses were done on ELSB11-D1 (A), ELSB11-D2 (B), ELSB11-D7 – D10 (F-I). The late Holocene section is represented by cores A and B and the early Holocene section is represented by cores F – I. Mazama ash can be seen in the ELSB11-D7 (F) as a dark gray layer. Laminations can be seen in the second half of core ELSB11-D8 (G) and all of ELSB11-D9 (H).

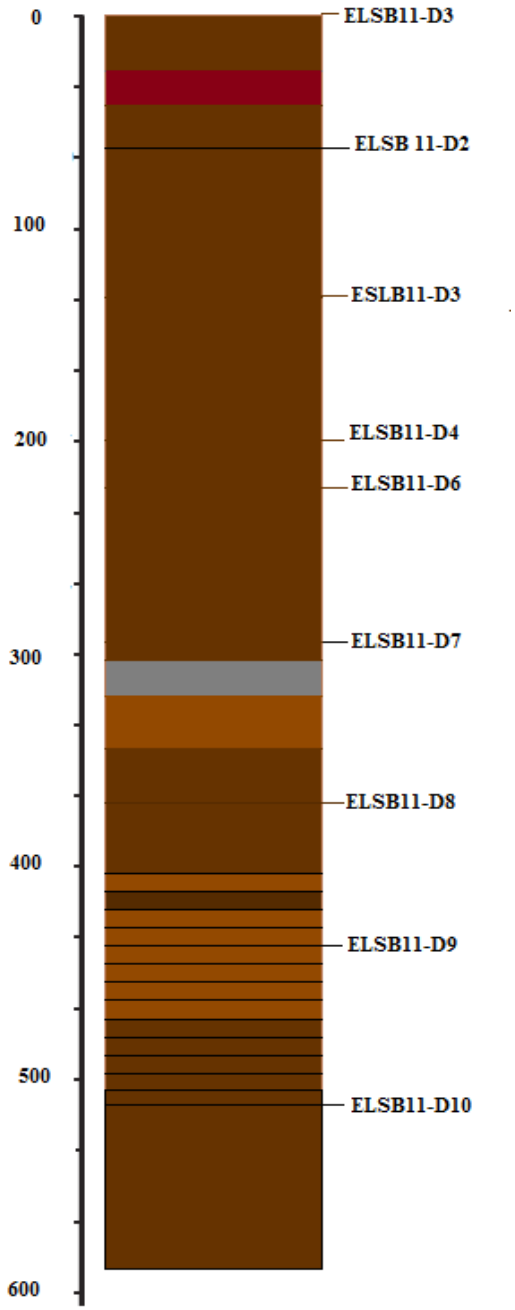

FIGURE 12. Stratigraphic column of ELSB11. ELSB11 color correspond to the Munsell color chart and is separated by drives. Gray bar represents Mazama tephra depostion, red bar is an unknown reddish brown layer seen in upper section of the core and repeating black lines represent diatomaceous laminations.

10 and 20 %TOC. The TOC shows significant variations, but there are no long-term trends besides the difference in amount of TOC between the two Holocene sections (Figure 13).

C:N Ratio

The C:N ratios show significant short and long-term variations. During the earliest part of the Holocene in ELSB11 (590 – 520 cm), the C:N ratios are very low (6-8), falling within a purely algal field. During the early Holocene (519 – 470 cm; diatomaceous laminations) there are more pronounced variations, but overall C:N is high (10 – 14) falling within the mixed algal/terrestrial field. From 470 cm to the Mazama ash tephra deposition, C:N ratios are low (6-8) again falling back into the algal field (Figure 13).

The late Holocene section shows little to no fluctuations. From 130 to 45 cm, C:N ratios are high (10-12) falling within a mixed algal/terrestrial field, then decrease from 44 to 0 cm within the algal field (Figure 13).

Normal-Alkane Distribution

Four samples from 595, 560, 496, and 478 cm were analyzed to represent the early Holocene (Figure 13). At 595 cm, the most abundant carbon chain is C29 with an overall Paq value of 0.57, indicating an emergent macrophyte signature. At 560 cm, the most abundant carbon chain is C23 with an overall Paq value of 0.74, indicating an algal signature. At 490 cm, the most abundant carbon chain is C29, with a Paq value of 0.47, indicating an emergent macrophyte signature. At 478 cm depth, the most abundant carbon chain is C29, with a Paq value of 0.57, indicating an emergent macrophyte signature.

Four samples from 96, 76, 18, and 0 cm (Figure 13) were also analyzed to represent the late Holocene. At 96 cm, the most abundant carbon chain is C23, with an overall Paq value of 0.81, indicating an algae signature. At 76 cm, the most abundant carbon chain is C23, with an

overall Paq value of 0.65, indicating an emergent macrophyte signature. At 18 cm, the most abundant carbon chain is C23, with an overall Paq value of 0.71, indicating an algal signature. At 0 cm, the most abundant carbon chain is C29, with an overall Paq value of 0.61, indicating an emergent macrophyte signature.

Biogenic Silica

During the early Holocene, from 600 to 545 cm depth, the wt. % BSi percentage ranges from 9 to 11 %. Within the diatomaceous laminations (550 – 425 cm), wt. % BSi percentages are at their highest values with a maximum of 12.5 %BSi. From 432 to 300 cm, wt. % BSi percentages decrease to a range of 5 – 9 wt. % BSi. The late Holocene section has little to no fluctuations and a constant wt. % BSi percentage ranging from 3 to 5 wt. % BSi (Figure 13).

Interpretations

Multi-Proxy Analyses for Eagle Lake Holocene Climate Change

All proxies (n-alkane distribution, TOC, C:N and wt. % biogenic silica) seem to be in a broad general agreement during the early Holocene. They indicate a productive, moderately nutrient-rich lake water with a high input of terrestrial organic source matter and mixture of emergent macrophytic/algal environments. The combination of high BSi and low %TOC suggests a productive system in which the organic carbon is readily respired. This would be consistent with a shallower lake that is prone to wind-driven mixing and less prolonged periods of anoxia in the hypolimnion. This model is also consistent with generally high C:N ratios between 9.4 and 8.4 cal ka BP (Figure 13). In general, the n-alkane data fall within the emergent macrophytic zone and thus also suggest that the southern basin was shallower than today. It is important to point out, however, that the same signature might also result from a mixture of algae and terrestrial carbon sources. The main feature of the early Holocene, regardless of the proxy, is

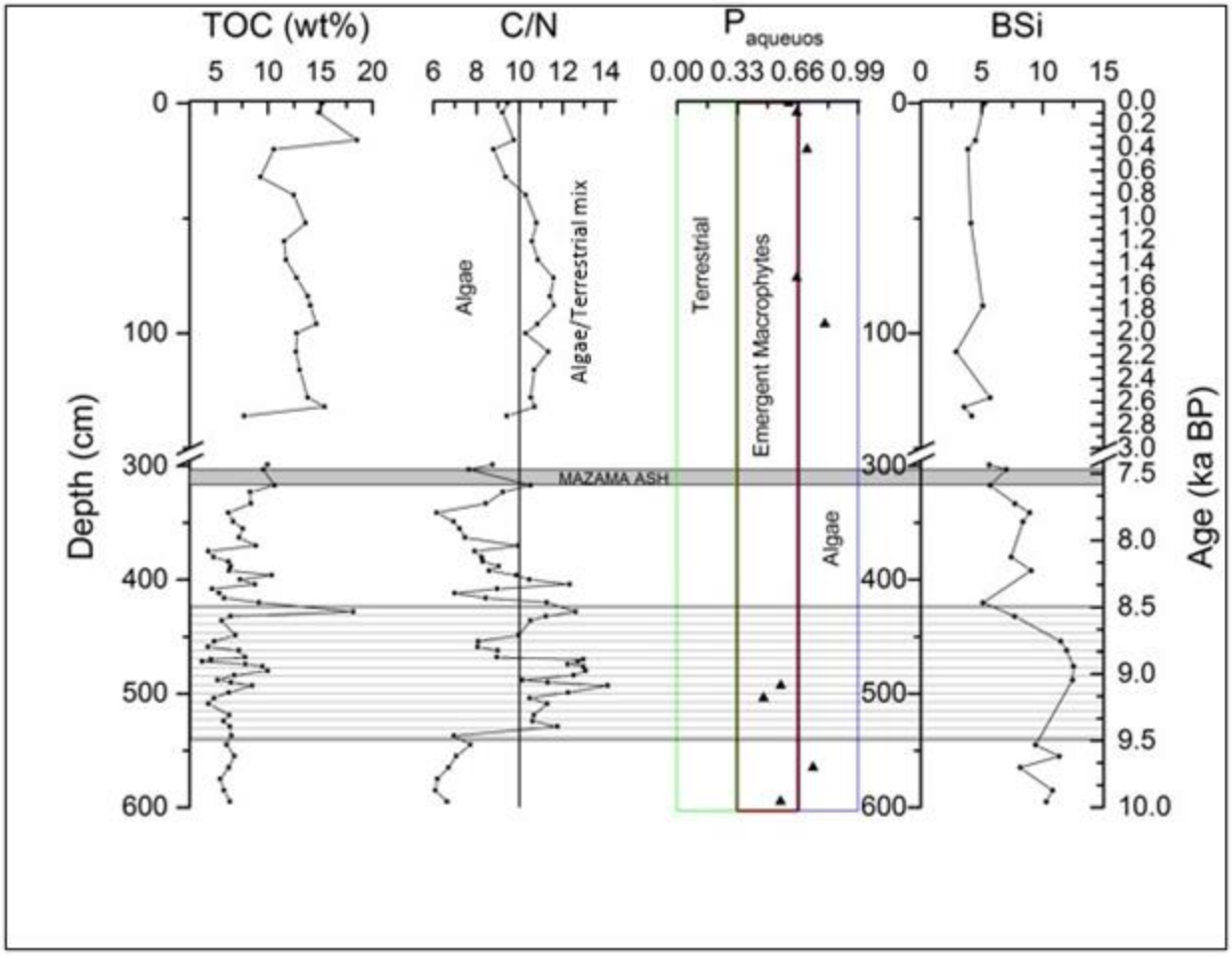

FIGURE 13. Proxy analyses of ELSB11 late Holocene and early Holocene. TOC, C:N ratios, Paqueous values from normal-alkane distribution (green rectangle indicates a terrestrial signature, red indicates an emergent macrophyte signature, blue indicates an algae signature) and BSi wt. % on right panel. Left y-axis plots depth (note break at ~300 cm) and right y-axis represents estimated age depth correlation with uncertainty in the late Holocene due to suspected slumps. Gray bar represents the Mazama ash and line marks represent diatomaceous laminations. Break in both axes indicate a separation between the late Holocene section and early Holocene section of ELSB11.

the great variability. For example, in the early Holocene, there is a prominent transition from a clear emergent macrophyte signature to an algal signature at ~9.8 – 9.6 ka BP.

In contrast, the late Holocene has much higher TOC levels and lower BSi, suggesting high levels of productivity in which the organic matter was preserved. This may be interpreted as an indication of Eagle Lake's ability to stratify and maintain anoxic bottom waters for much of the year. However, during the late Holocene, the C:N ratios are within the mixed algal/terrestrial zone until the upper 20 cm. In contrast Paq values plot in the algal source region. Thus, Paq is consistent with a deeper lake dominated by algae. Although C:N ratios of 10-15 are often interpreted as being derived from emergent macrophytes, such ratios can be a combination of algal and terrestrial organic matter transported to the lake by wind or water. Thus the late Holocene C:N ratios may indicate a higher amount of runoff, which may be consistent with more snowpack.

NAPD Transition Zone at Eagle Lake

The current climate regimes of the western US indicate that on multi-year times scales, Eagle Lake falls in the transition zone between the dry PSW and wet PNW. However, if the transition zone moves north and south, Eagle Lake may fall within either the PSW or PNW. During the earliest Holocene, prior to 10 ka BP, low C:N, low TOC and the n-alkane data suggest algal dominance of the organic matter. This result is interpreted as indicating high lake levels, which places Eagle Lake in the PSW climate regime. This shift puts the transition zone to the north of Eagle Lake (Figure 15). This result is consistent with the northward penetration of the North American monsoon. However, this effect was not long-lived as the boundary moved southward after several hundred years.

Around 10 ka BP, the NAPD transition zone migrated south of Eagle Lake. From ~10 to 8 ka BP, the increase in C:N ratios, shift to terrestrial n-alkanes, and abundance of benthic diatoms (Weide, M., pers. comm., 2017) suggest lower lake levels and enhanced aridity—placing Eagle Lake in the PNW climate regime (Figure 14). Given that Pyramid Lake, only 120 km to the south likely falls in the PSW regime at this time, the transition zone has been narrowly confined during this interval.

During the late Holocene, the increase in TOC, algal dominated n-alkanes and low C:N ratios indicate deeper water and an overall wet climate. In the late Holocene, Eagle Lake continues to have a climatic affinity with the wet PNW, and the transition zone is still located south of Eagle Lake.

Current Conditions in the Southern Basin

The late Holocene record in the southern basin would be easier to interpret if the last 100 years of known lake level changes were preserved. However, the Lassen Peak ash, prominent in core ELBB16, is missing in the southern basin, suggesting that the ash and the sediment above it slumped to deeper depths. This may have occurred during the 1922 earthquake (Roberts and Gross, 1982) which had an epicenter under Eagle Lake. Regardless of the missing time, the late Holocene record does show distinct differences from the early Holocene sediment record.

Conclusion

The earliest Holocene shows evidence of a deep, algal dominated lake, consistent with the wet PSW and the northward penetration of the North American monsoon. However, by 10 ka BP, lake level dropped indicating a southward shift in the NAPD boundary. Wetter intervals occurred during the earliest Holocene but the timing of them is not well constrained. The late Holocene record lacks the last 100 years for comparison, but it appears to have been

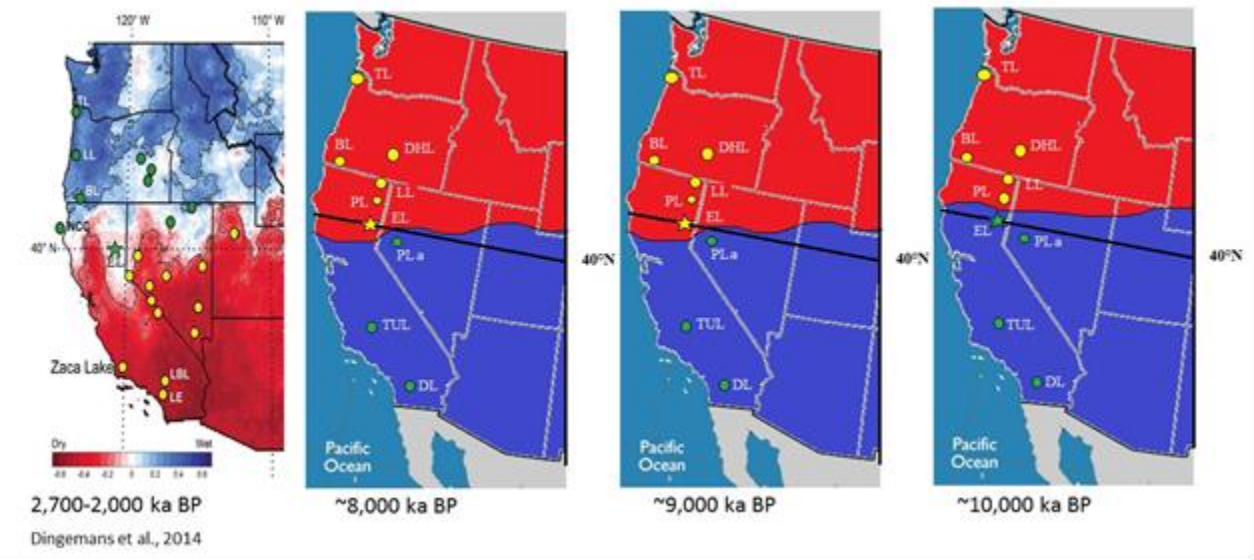

FIGURE 14. Regional comparison of Eagle Lake dynamic through time. Eagle Lake shown as a star. Green stations indicate a wet climate and yellow stations indicate a dry climate. The background shows correlation coefficients between Jun-Nov SOI and Oct-Mar precipitation. Negative values shown in red and represent dry climate, positive blue values represent wet climate. * NAPD transition zone migrating northward or southward during each Holocene phase. TL = Tulane Lake, BL = Bolane Lake, DHL = Dead Horse Lake, LL = Lily Lake, PL = Patterson Lake, PLa = Pyramid Lake, EL = Eagle Lake, TUL = Tulare Lake, DL = Dry Lake (Source: panel on far left from Dingemans et al., 2014).

wetter (or as wet) as today. The NAPD boundary remained south of Eagle Lake throughout the late Holocene. In fact, Eagle Lake tends to fall within the PNW climate regime throughout most of the Holocene. However, comparing Eagle Lake with other sites, it is clear that the transition zone is always proximal.

CHAPTER 4

THE LAST 100 YEARS AT EAGLE LAKE

Both climatic change and anthropogenic modification marked the last 100 years at Eagle Lake. Lake level varied significantly from 1910 - 2010 (Aubrey, V., pers. comm., 2015). Compared to recent levels, the lake level was much higher between 1910 and -1920, with an average elevation of 1563 m above sea level. By comparison, the 2017 lake level elevation was 1553 m, 10 m lower than the historical high level in 1910. The cause of this major drop in lake level is likely a combination of natural climate variability and the construction of the Bly Tunnel. Is it possible to discern natural lake level drop from the human-induced one in the sedimentary record? This chapter focuses on the sedimentary record of this period with an aim to determine if these two impacts can be disentangled.

Human Impacts

Eagle Lake has long been considered a potential source of water for the arid Honey Lake Valley. The earliest attempt to tap the lake occurred in AD 1875 (Purdy, 1988). The Lassen Flume and Land Company tried to drill a tunnel to the lake, but failed from lack of finances. In 1891, plans were developed by the Eagle Lake Land and Irrigation Company to pump water into neighboring creeks. Water was pumped for a few months, but this project failed as well. The last attempt to develop a water supply from the lake was made by Leon Bly. His plan involved the construction of the Bly Tunnel to transport water from Eagle Lake to Willow creek. In 1921, work commenced on the 7300-foot tunnel from Murrers Upper Meadow toward the lake (Figure 15). Water was to enter Willow Creek and then be redirected through a series of canals, flumes, and siphons to farms in Honey Lake Valley. In the beginning, the plans called for the tunnel to tap the lake at ~45 feet below the lake surface at the time. However, a zone of

excessive subsurface seepage was encountered 300 feet from the lake during construction of the tunnel. As a result, tunnel construction halted and modifications were made to the inclination of the tunnel, slanting it at a higher degree to compensate for the drop in lake level and inserting a 60-inch corrugated metal pipe (Purdy, 1988).

From 1923 to 1935, water flowed continuously into the tunnel, and lake level dropped by an estimated 27 feet. Concurrently, the western US was experiencing a major drought (1920s-1930s), which likely also contributed to the drop in lake level. Decreases in lake level caused the inlet channel of the Bly tunnel to constantly be deepened. Lake levels dropped so drastically that there was not enough water to reach the inlet from 1940 to 1949. In the summer of 1955, lake levels had recovered filling the intake channel, but an "unknown group of citizens" filled the tunnel with sand, cutting it off from the lake (Purdy, 1988). By 1977, the Bureau of Land Management installed a permanent concrete plug half way through the tunnel that allowed five cubic feet per second of water to flow through in accordance with the State of California. Water flowed continuously until the Department of Fish and Game asked the State Water Control Board in 2012 to close the bypass pipe, officially closing off the continuous flow of water into the Bly tunnel. Despite this effort, the lake level has not recovered its historic peak levels.

Climate Change over the Last 100 Years

The Palmer Drought Severity Index (PDSI) uses temperature and precipitation data to estimate relative dryness of a particular region. It is a standardized index that spans a range of -10 (dry) to +10 (wet). The PDSI for the Eagle Lake region shows six intervals with severe drought lasting a minimum of 3 years (Figure 16): 1917-1941 (Dustbowl), 1947-1955, 1959-1962, 1975-1981, 1988-1995, and 2002-2016. Based on the reconstructed PDSI, there was a shift from exceptionally wet to dry conditions around 1915 in this region, well before the onset of the

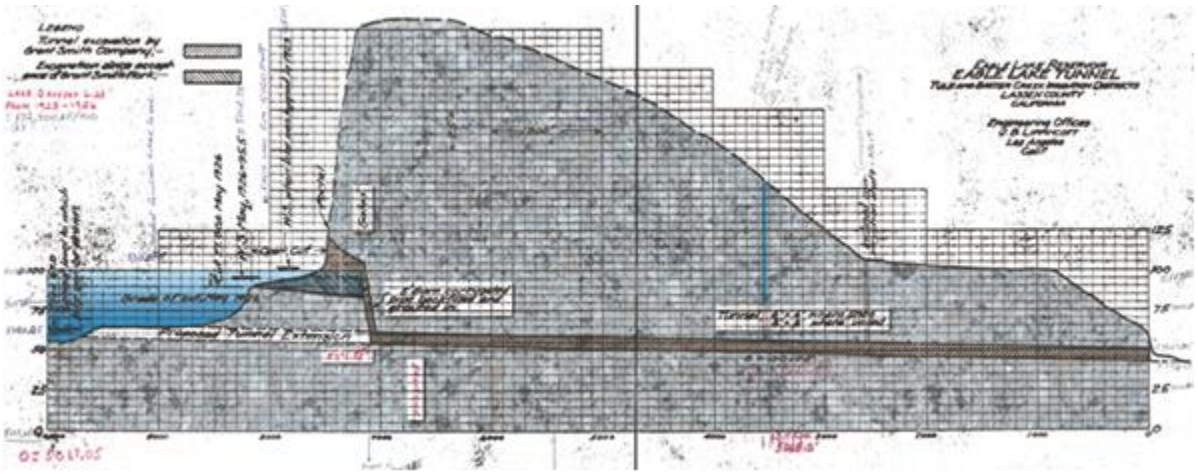

FIGURE 15. Detailed plans of the Bly Tunnel after completion. Shown is also the improvised cut that was proposed because of lake level drop and the 2600 foot mark access tunnel where tailings of the tunnel were taken out (from Bateson, 2016).

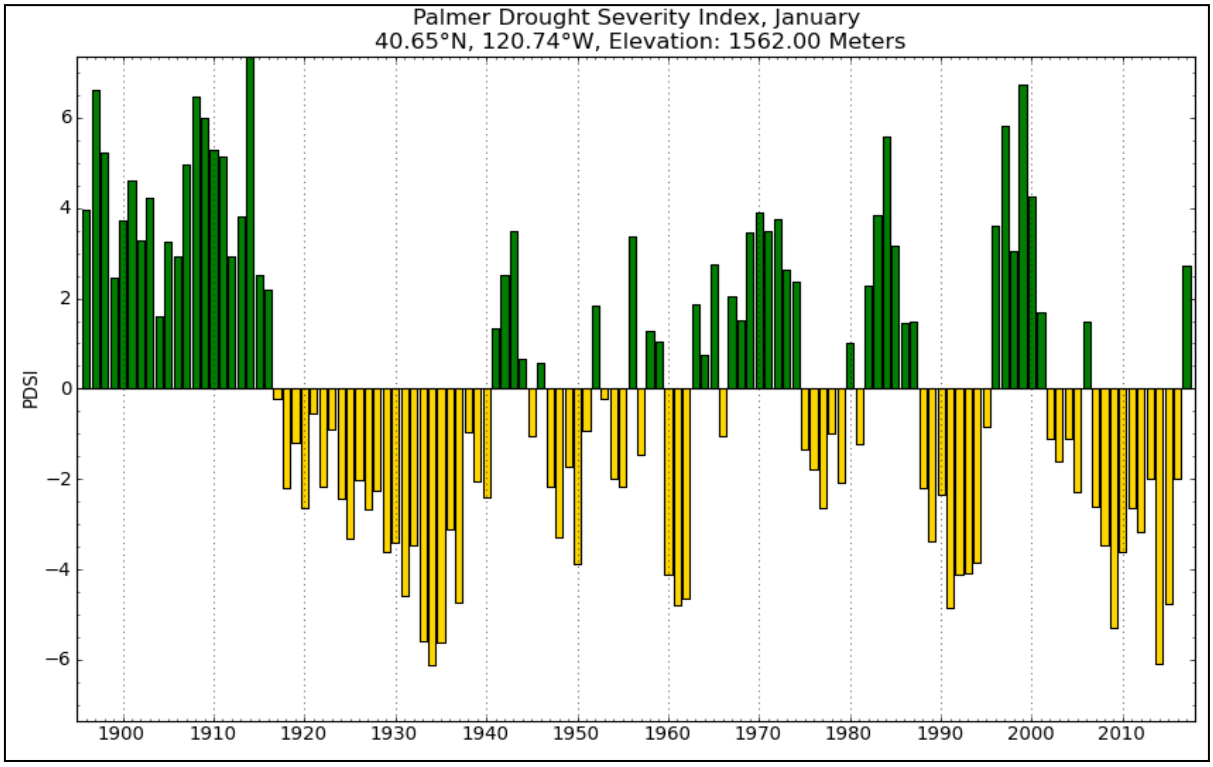

FIGURE 16. Palmer Drought Severity Index over Eagle Lake from 1900-2017. PDSI ranges from dry (negative, yellow) to wet (positive, green) values. Values are indications above or below the averages. (from Western Regional Climate Center).

classical Dust Bowl drought of the 1930s. However, the drought intensified over the next two decades reaching extreme levels by the mid-1930s. The spatial extent of this drought was large, stretching from the Great Plains from the Gulf of Mexico into Canada and much of the Pacific Northwest (Figure 17).

Comparison Between Lake Level Variation, Climate, and the Bly Tunnel

Lake level closely tracks the PDSI (Figure 18), although there are lags between the forcing (PDSI) and response (lake level). Prior to the 1915 Lassen Peak eruption, lake levels were at the highest recorded at 1563 m elevation. These levels persisted for about 10 years, but available moisture had already begun to decrease and in 1917 the drought officially began. The lake level lagged behind the PDSI drought, but slowly began to drop to its lowest level of 1552 m elevation in 1938. In the midst of the drought which initially caused a ~ 3 m drop in lake level, the Bly Tunnel withdrawal was initiated lasting from 1923 to 1935. Figure 18 shows the PDSI drought, Eagle Lake levels, and the active period for the Bly Tunnel. Although the lake level was clearly dropping by this time, the precipitous drop by 8 m during this time may be linked to the activity of the Bly Tunnel.

In an effort to maintain water flow to the tunnel, Bly had to continuously deepen the intake canal (Purdy, 1988). After the tunnel was abandoned, the timing of lake level variations couples closely with the PDSI, although a persistent lag in lake level change is obvious. What is of interest is the magnitude of the PDSI variations are not matched by lake level. For example, 1997-2001 were some of the wettest years on record in the last 100 years, yet the lake level is lower than it was during the previous wet interval in the 1980s.

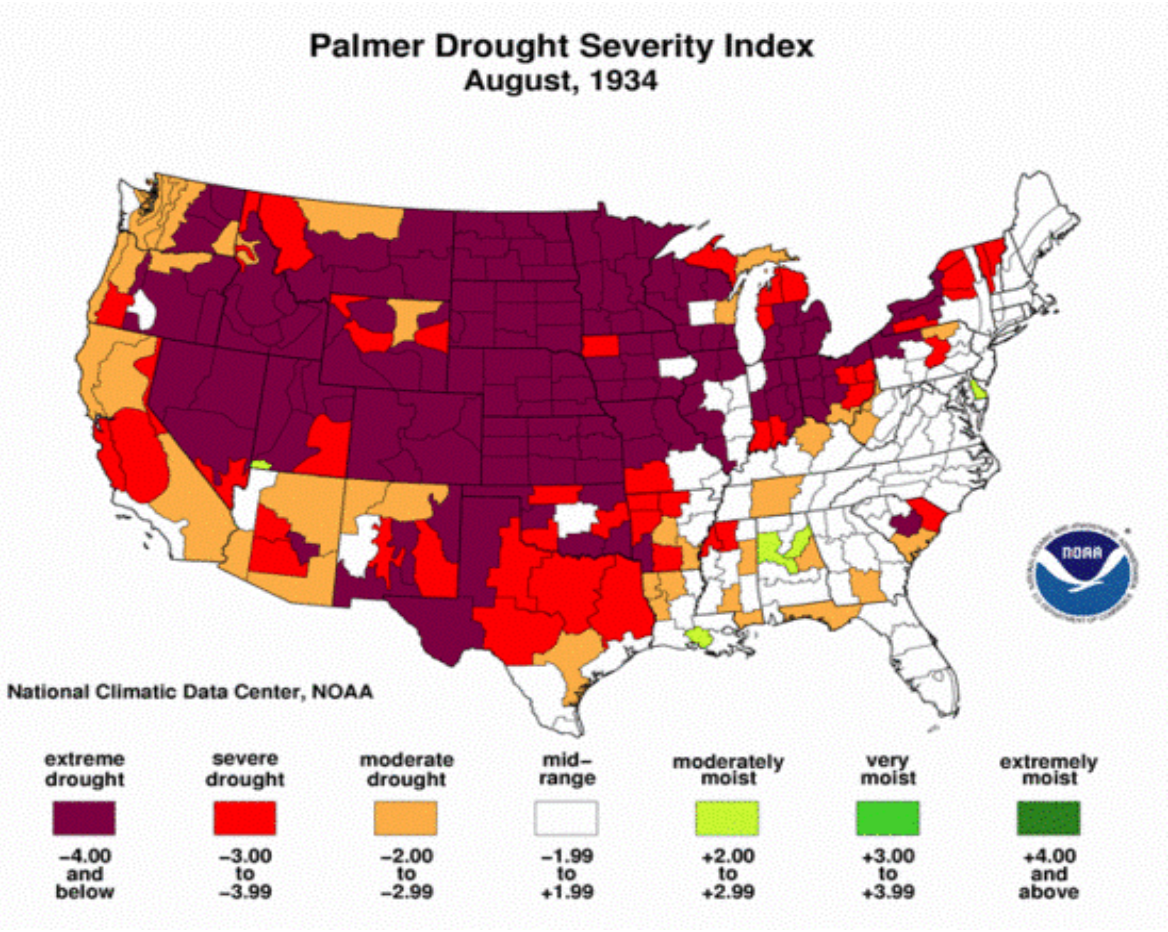

FIGURE 17. Map showing the Palmer Drought Severity Index, August 1934 (from NOAA).

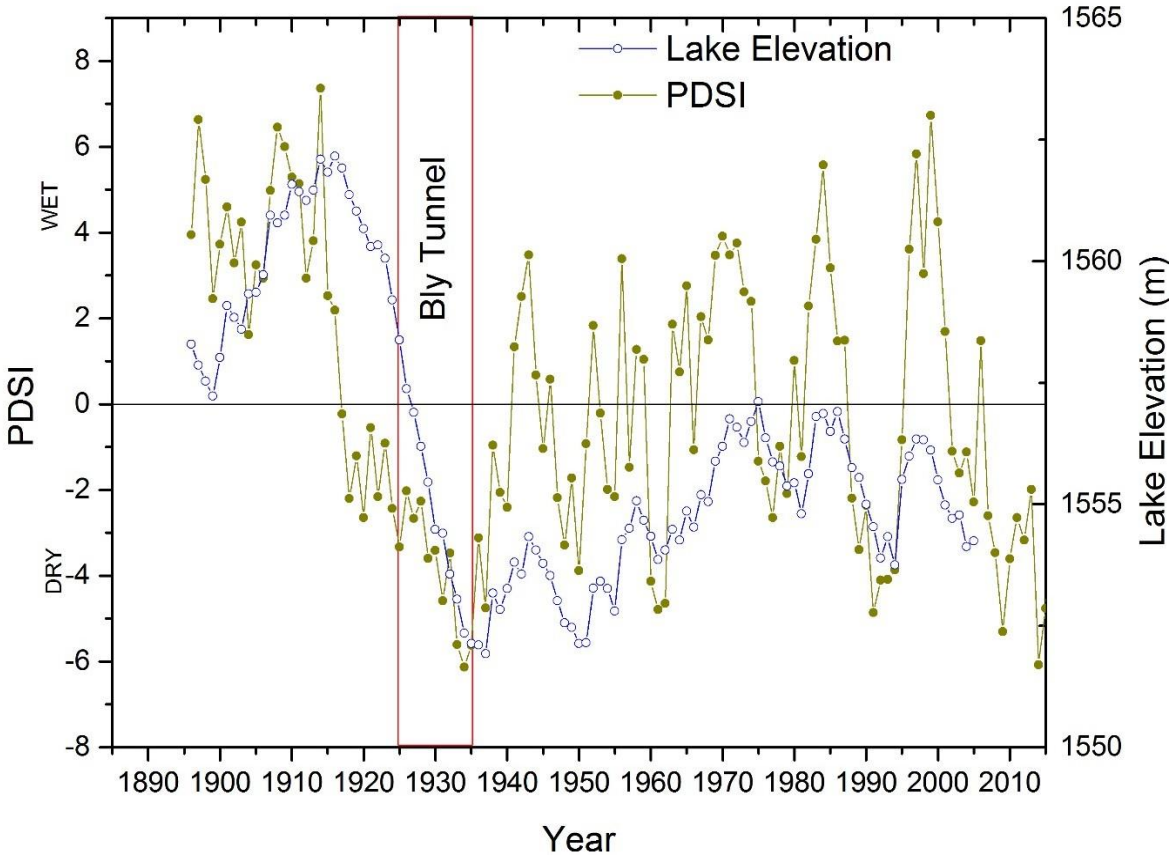

FIGURE 18. Palmer Drought Severity Index for Eagle Lake, CA overlain Eagle Lake water level through time. (PDSI data from Western Regional Climate Center; lake level data from Bateson, 2016).

Results

Core Lithology

The sediment from the last 100 years comes from Bucks Bay (ELBB16), a shallow inlet with a current water depth (as of spring 2016) of ~1 meter. The sediment is a brown gyttja below the Lassen Peak ash layer. Above the ash, the sediment becomes lighter and numerous ostracodes and some gastropods can be seen in the sediment. A stratigraphic profile showing the main features is shown in Figure 19 and the Munsell color designations in Table 3.

Age Model

Radiocarbon dating was not attempted on the Bucks Bay core due to large calibration errors from radiocarbon plateaus in the last 300 years. However, a tephra layer at 99 cm depth is tentatively correlated to the Lassen Peak eruption in AD 1915 (Clynne, 1999) (Figure 20). The average sedimentation rate is estimated at ~1.1 cm/year. Using a constant sedimentation rate, a tentative chronology is applied to the record (Figure 21).

Total Organic Carbon

There is a clear trend in TOC with generally lower values in the lower part of the core and higher values in the upper part of the core. From 180 to 85 cm, the %TOC ranges from 0 to 5 %TOC with a gradual transition to a higher range of 10 – 15 %TOC after 85 cm (Figure 21).

C:N Ratios

C:N ratio data range from 10 to 15. There is a slight decrease below the Lassen Ash and a small increase between 1920 and 1940. The low value at 99 cm contains ash and is highly diluted in organic matter (Figure 21).

N-Alkane Distribution

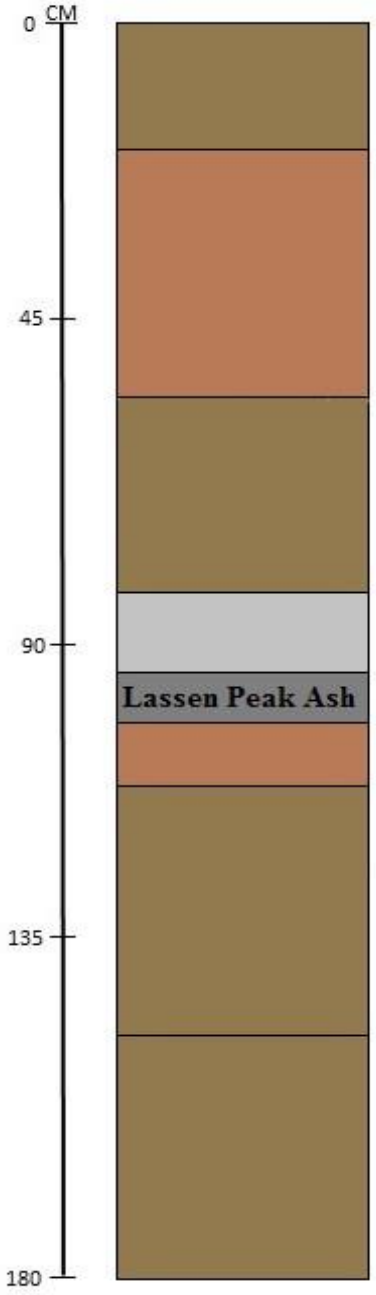

FIGURE 19. Stratigraphic column of ELBB16.

TABLE 3. Munsell Color Scheme for ELBB16

Core	Depth (cm)	Munsell Color	Color Notation	
ELBB16	0 - 15	Dark yellowish brown	10 YR 4/2	
	16 - 26	dusky yellow brown	5 YR 4/2	
	27 - 72	Dark yellowish brown	10 YR 4/2	
	72 - 97	Light olive gray	5Y 5/2	
	98 - 100	Medium light gray	7 N7	(Lassen Peak Ash)
	101 - 120	dusky yellow brown	5 YR 4/2	
	121 - 144	Dark yellowish brown	10 YR 4/2	
	145 - 180	pale yellowish brown	10 YR 6/2	

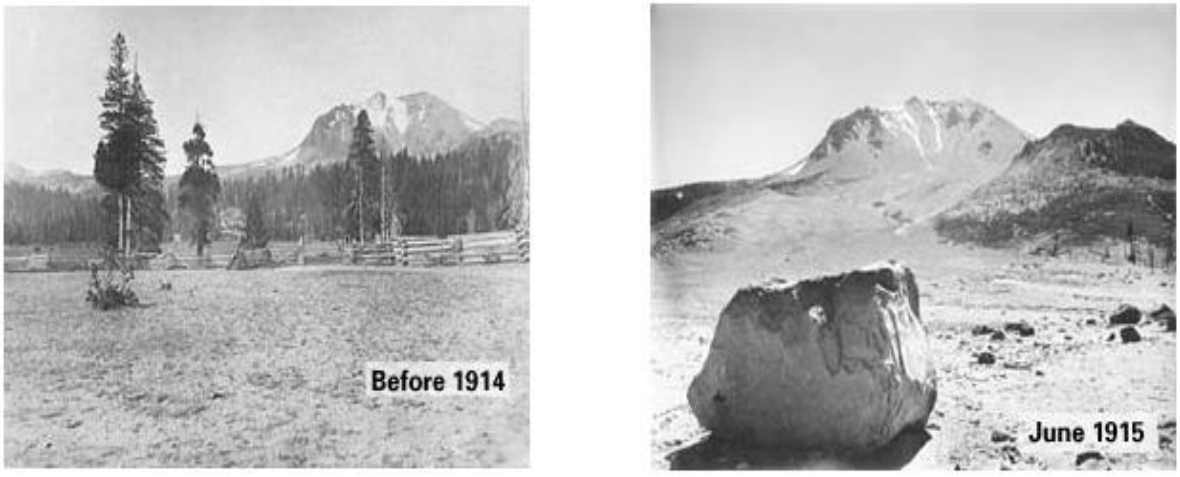

FIGURE 20. Series of explosive eruptions at Lassen Peak. Photograph on left is the northeastern flank of Lassen Peak covered by mature conifer forest before 1914. Right photograph is the same location in June 1915 (from U. S. National Park Service).

Two samples at 84 and 25 cm were also analyzed for n-alkane distribution. At 84 cm, the most abundant carbon chain is C25, with a Paq value of 0.64, indicating an emergent macrophyte signature. At 25 cm, the most abundant carbon chain is C25, with a Paq value of 0.64, also indicating an emergent macrophyte signature (Appendix D). The data are not shown on Figure 21.

Biogenic Silica

The wt. % BSi record has consistently high values from 140 to 40 cm (~1880-1970). However, the record also has significant variation in this interval with values ranging between 5 and 9 wt. % BSi. From 40 to 0 cm (~ AD 1970 to present), the BSi record has lower values, which are uniform at ~ 4 %BSi (Figure 21).

Discussion

A direct comparison of the lake level and the PDSI suggest that lake began to drop prior to the opening of the Bly Tunnel. Water level decreased by ~2 m in the first years of the drought but the intensification of the drought was simultaneous with the tunnel and the further decrease in lake elevation cannot be disaggregated between the two factors. The sedimentary record cannot be directly compared to decadal variations in lake level without more precise dating. However, general trends can be documented and the tentative chronology allows for a coarse comparison. According to the PDSI, ~1900 – 1917 was a wetter-than-average interval. During this time period, Eagle Lake water levels were at their highest. The corresponding sediment is a dark green gyttja with few ostracodes, suggesting deeper water than today. Low C:N ratios suggest a mix of algal and terrestrial organic sources, which is not surprising given the close position of the core to the shore. The high wt. % BSi indicates that nutrients are readily available to Bucks Bay, regardless of the water level.

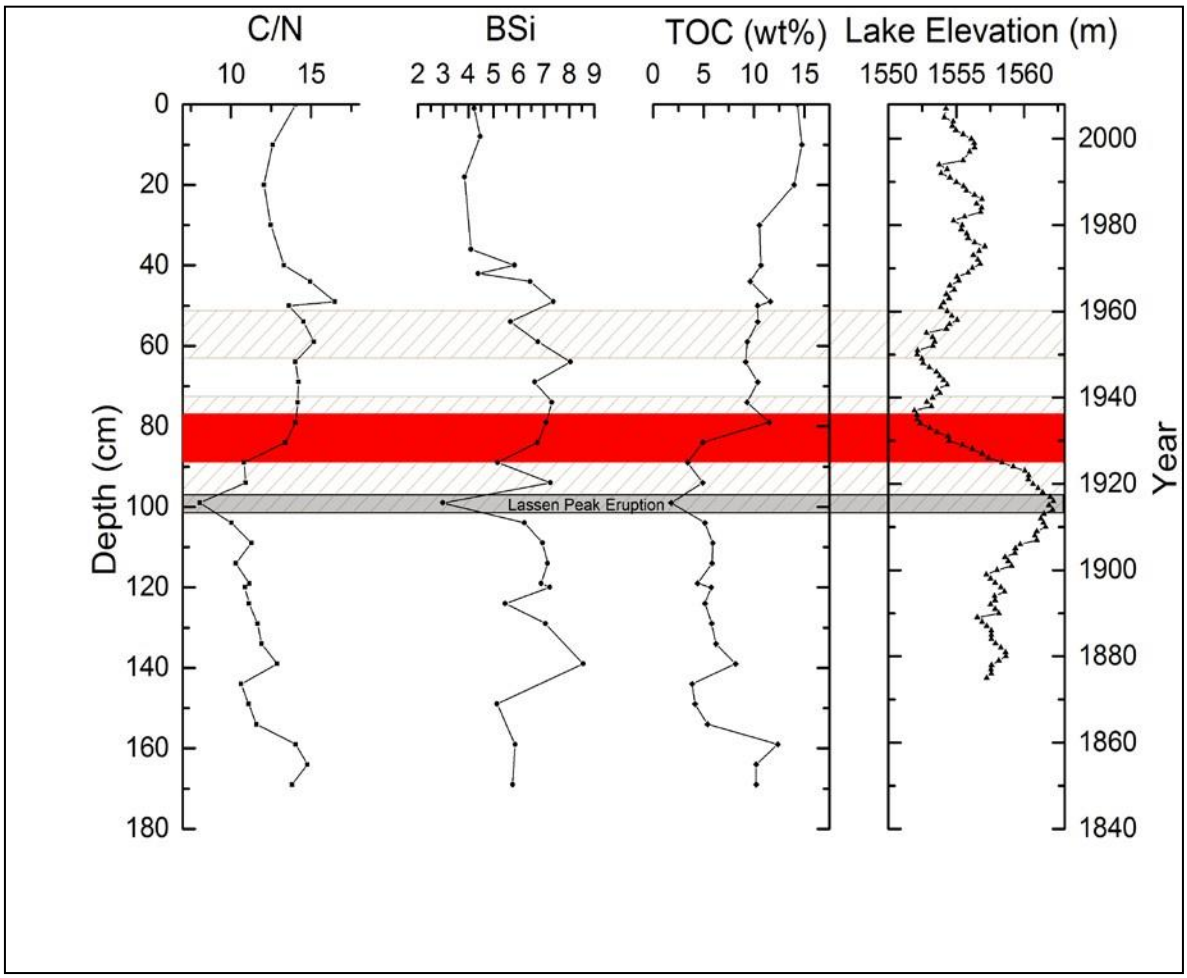

FIGURE 21. C:N, BSi, and TOC for ELBB16 with depth on the left axis and a tentative age on the right axis. Far right panel is lake level elevation of Eagle Lake for the past 100 years (from Lassen County Public Works). Gray bar represents the 1915 Lassen Peak eruption. Brown hatch marks represent years of drought based on the Palmer Drought Severity Index. Red bar represents period the Bly Tunnel was most active.

From ~1920 – 1940, climate was excessively dry. During this time period, Eagle Lake water levels declined drastically. Some of the initial drop was clearly climate related, but the opening of the Bly Tunnel clearly exacerbated the water loss. Although the C:N ratios show gradual increase, %TOC has a more abrupt increase during the height of the drought. Both may indicate greater contributions of submerged macrophytes as the level dropped and the photic zone intersected the sediment. Unfortunately, neither is able to disentangle the natural from human-induced factors. The increase in macrophytes that contribute to both the C:N and %TOC provided food and shelter for ostracodes that rapidly increase in abundance as lake level fell.

The biogenic silica record may indicate changes in productivity. The cause of such changes is usually related to nutrient loading through either wind-induced mixing (Johnson et al., 2002) or anthropogenic nutrient enrichment (Conley and Schelski, 2001). Silica is not a limiting nutrient given that the geology of Eagle Lake consists of silicate rocks. Therefore, the wt. % BSi is likely an indication of overall productivity. Because there is no correspondence of BSi to drought periods, evaporative concentration of key nutrients is not a factor. It is possible that winds during the low stands mixed nutrients allowing for more diatom blooms. After 1970, when lake levels rose slightly, such mixing may have been slightly reduced. It is also possible that after 1970, the installation of septic systems in homes around the lake reduced the sewage input (Schelske et al., 1986). Thus, it is hypothesized that high values of wt. % BSi from 1880 – 1940 occurred because diatom production was stimulated by phosphorous enrichment through sewage.

Conclusions

During the last 100 years, it is clear that Eagle Lake levels were at their highest prior to the Lassen Peak eruption. From 1920 to 1940 water levels dropped and can be attributed to both climate and human-induced factors. Although the sedimentary record cannot discern the

difference between the two, the sediment does track the variations in lake level with lower C/N and TOC and few ostracodes with high lake levels. These observations are consistent with the interpretation of lake level in the southern basin during the Holocene.

CHAPTER 5

FUTURE WORK

To disentangle the effects of the drought and the tunnel, it may be useful to use stable isotopes of carbonates. Stable isotopes will increase in response to the drought as 16O is preferentially removed by evaporation. The same response will not happen if lake level drops via surface outflow (e.g., the tunnel). The best source of isotopic analysis is ostracodes. Ostracodes precipitate their shells from ions taken directly from water, so ostracode carapace compositions reflect that of the host water chemistry.

Abundant ostracodes were found only in the Stone's Landing short core and the upper part of ELBB16. Two different ostracodes were found throughout the short core in quantities for isotopic analysis. They were both given names that highlight their features: "bumblebee" and "dog-nosed" (Figure 22). The bumblebee ostracod is likely Candona caudata, a species with a hook-shaped extension typically found in freshwater Mediterranean climates (Kaufmann, 1900). The other ostracode remains an unidentified species.

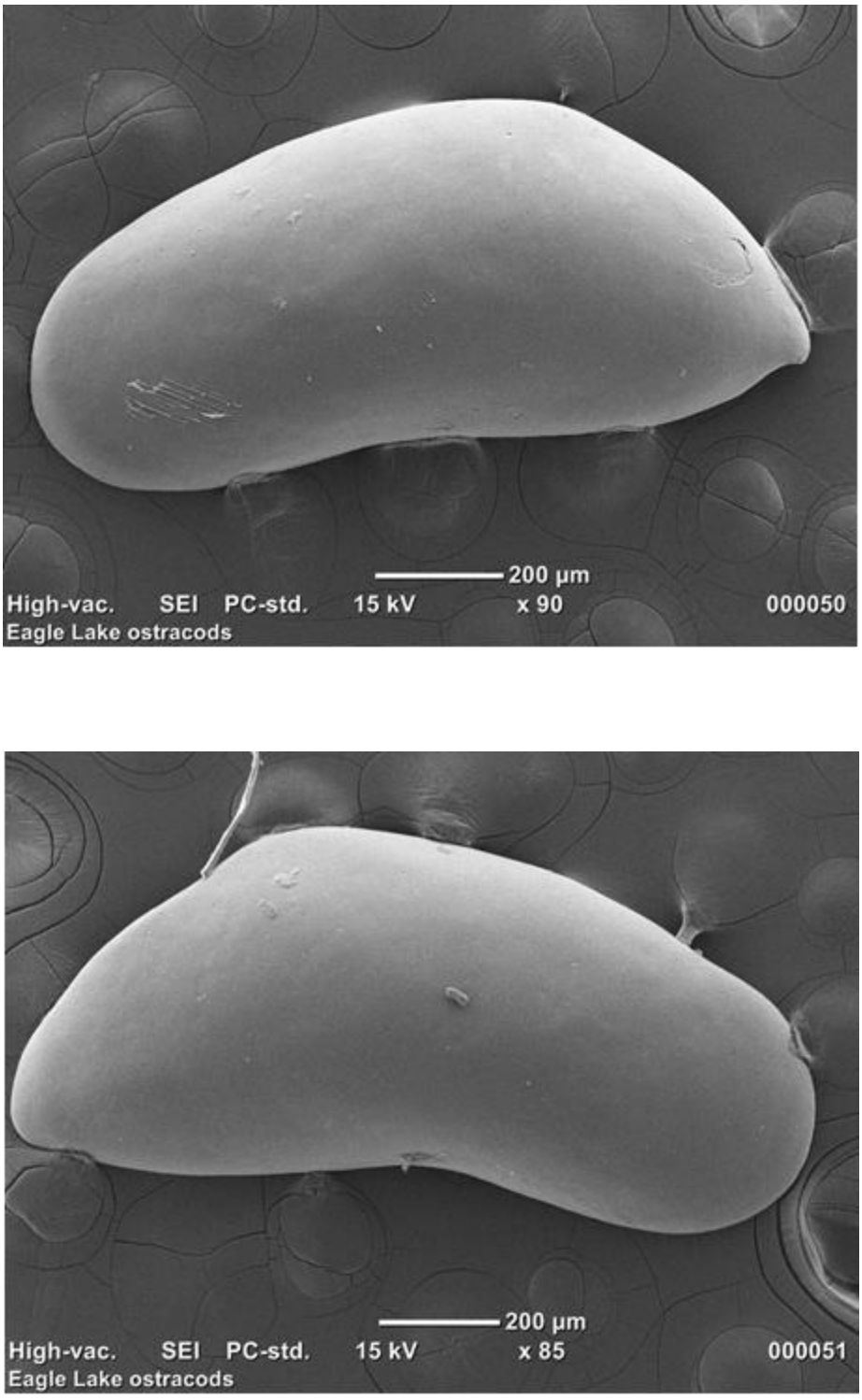

FIGURE 22. Scanning electron microscopy of ostracod species found in the Stone's Landing short core. Informally identified as "bumblebee" Candona caudata (top) and "dog-nosed" (bottom).

APPENDICES

APPENDIX A

TOTAL ORGANIC CARBON DATA

ELSB11-LATE HOLOCENE SECTION	True Depth (cm)	% TOC
	0	15.21
	4	14.82
	8	
	16	18.5
	20	10.56
	32	9.27
	36	
	40	12.45
	52	13.6
	60	11.53
	68	11.72
	76	12.75
	84	13.82
	88	14.06
	96	14.63
	100	12.75
	108	12.69
	116	13.03
	128	13.79
	132	15.41
	136	7.72

ELSB11-EARLY HOLOCENE	True Depth (cm)	TOC
	299	9.96
	303	9.56
	317	10.61
	323	8.3
	333	8.35
	341	6.22
	349	6.67
	355	7.57
	363	7.24
	370	8.83
	375	4.28
	380	4.78
	384	6.22
	388	6.42
	392	6.27
	396	10.33
	400	7.32
	404	8.75
	408	4.66
	412	5.32
	416	5.82
	420	9.13
	428	18.16
	432	6.4
	436	5.57
	449	6.87
	454	4.85
	459	4.27
	462	7.18
	468	7.79
	470	4.54
	472	3.69
	474	7.84
	476	9.46
	480	9.94
	484	6.76
	488	5.18
	490	6.45
	493	8.46
	499	6.25
	504	4.82
	509	4.29
	519	6.29
	524	5.73
	529	6.35
	537	6.47
	545	6.01
	555	6.78
	565	6.23
	575	5.44
	585	5.78
	595	6.36

ELBB16	True Depth (cm)	TOC
	0	14.31
	10	14.75
	20	13.99
	30	10.54
	40	10.35
	50	10.67
	60	9.33
	70	10.38
	80	11.51
	90	3.43
	100	1.78
	110	5.91
	120	5.75
	130	5.80
	140	8.17
	150	4.15
	160	12.36
	170	10.22

APPENDIX B

CARBON:NITROGEN RATIO DATA

ELSB11 - LATE HOLOCENE SECTION	True Depth (cm)	c:n
	0	9.447205
	4	9.204969
	16	9.736842
	20	8.8
	32	9.363636
	40	10.28926
	52	10.79365
	60	10.57798
	68	10.85185
	76	11.59091
	84	11.42149
	88	11.61983
	96	10.83704
	100	10.28226
	108	11.33036
	116	10.68033
	128	10.52672
	132	10.70139
	136	9.414634

ELSB11-EARLY HOLOCENE	True Depth (cm)	c:n
	299	8.736842
	303	7.648
	317	10.50495
	323	9.222222
	333	8.434343
	341	6.158416
	349	6.947917
	355	7.209524
	363	7.463918
	370	9.921348
	375	7.925926
	380	8.241379
	384	8.293333
	388	9.042254
	392	8.589041
	396	9.838095
	400	10.45714
	404	12.32394
	408	8.961538
	412	7
	416	8.434783
	420	11.2716
	428	12.61111
	432	11.22807
	436	10.50943
	449	9.956522
	454	8.083333
	459	8.056604
	462	8.975
	468	8.954023
	470	12.97143
	472	12.72414
	474	12.25
	476	12.9589
	480	13.07895
	484	12.51852
	488	10.15686
	490	11.31579
	493	14.1
	499	12.2549
	504	10.47826
	509	11.28947
	519	10.66102
	524	10.61111
	529	11.75926
	537	6.956989
	545	7.705128
	555	7.0625
	565	6.698925
	575	6.181818
	585	6.084211

ELBB16	True Depth (cm)	c:n
	0	14.02941
	10	12.60684
	20	12.49107
	30	14.43836
	40	13.61798
	50	13.8
	60	14.52055
	70	13.3662
	80	11.84146
	90	13.15854
	100	13.57609
	110	14.70408
	120	11.2381
	130	11.28571
	140	13.66304
	150	12.74699
	160	13.1625
	170	13.17442
	180	8.969697
	190	12
	200	9.046154

APPENDIX C

NORMAL-ALKANE DISTRIBUTION DATA

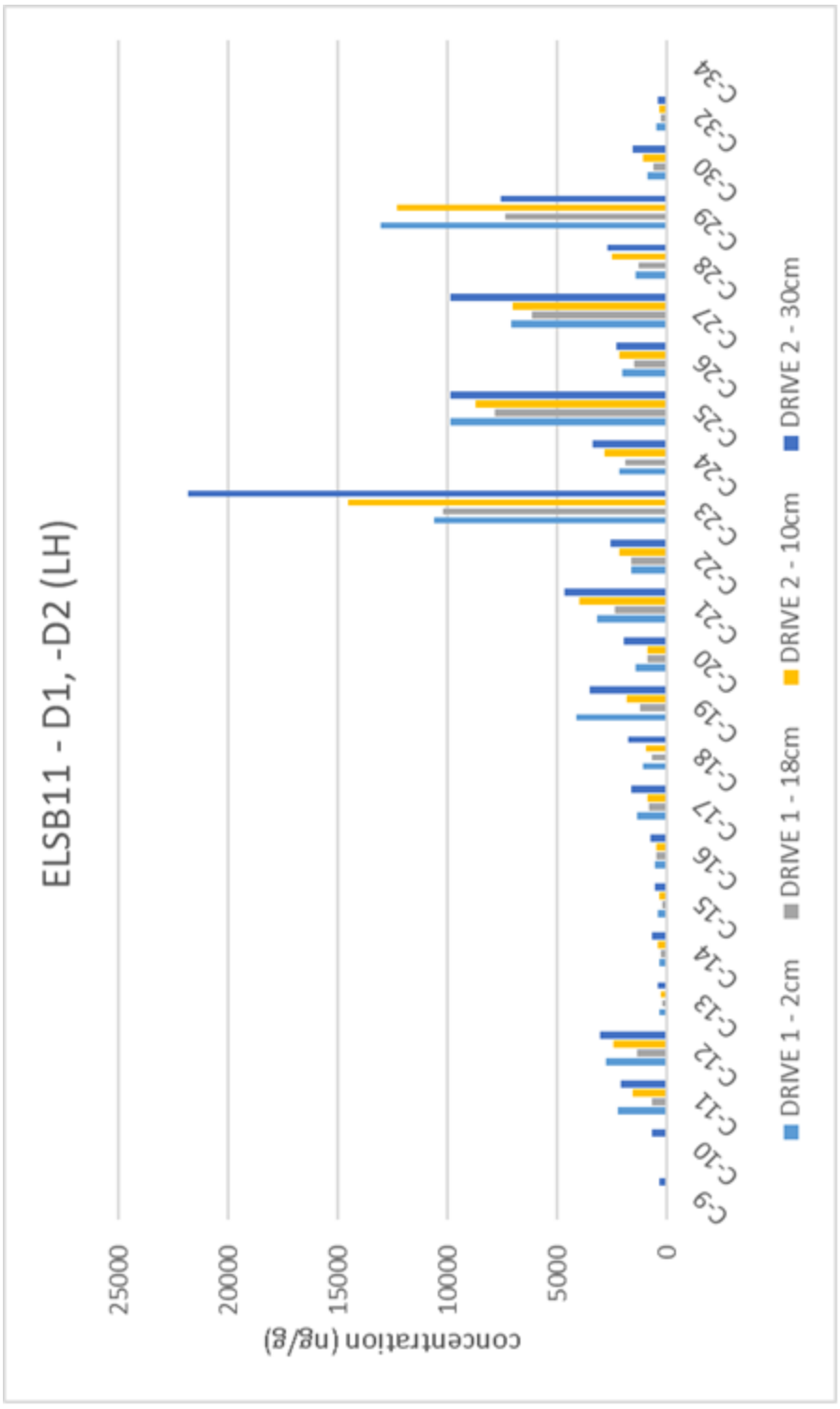
ELSB11 - D1, -D2 (LH)
concentration (ng/g)
25000
20000
15000
10000
5000
0
C9
C10
C11
C12
C13
C14
C15
C16
C17
C18
C19
C20
C21
C22
C23
C24
C25
C26
C27
C28
C29
C30
C32
C34
DRIVE 1 - 2cm
DRIVE 1 - 18cm
DRIVE 2 - 10cm
DRIVE 2 - 30cm

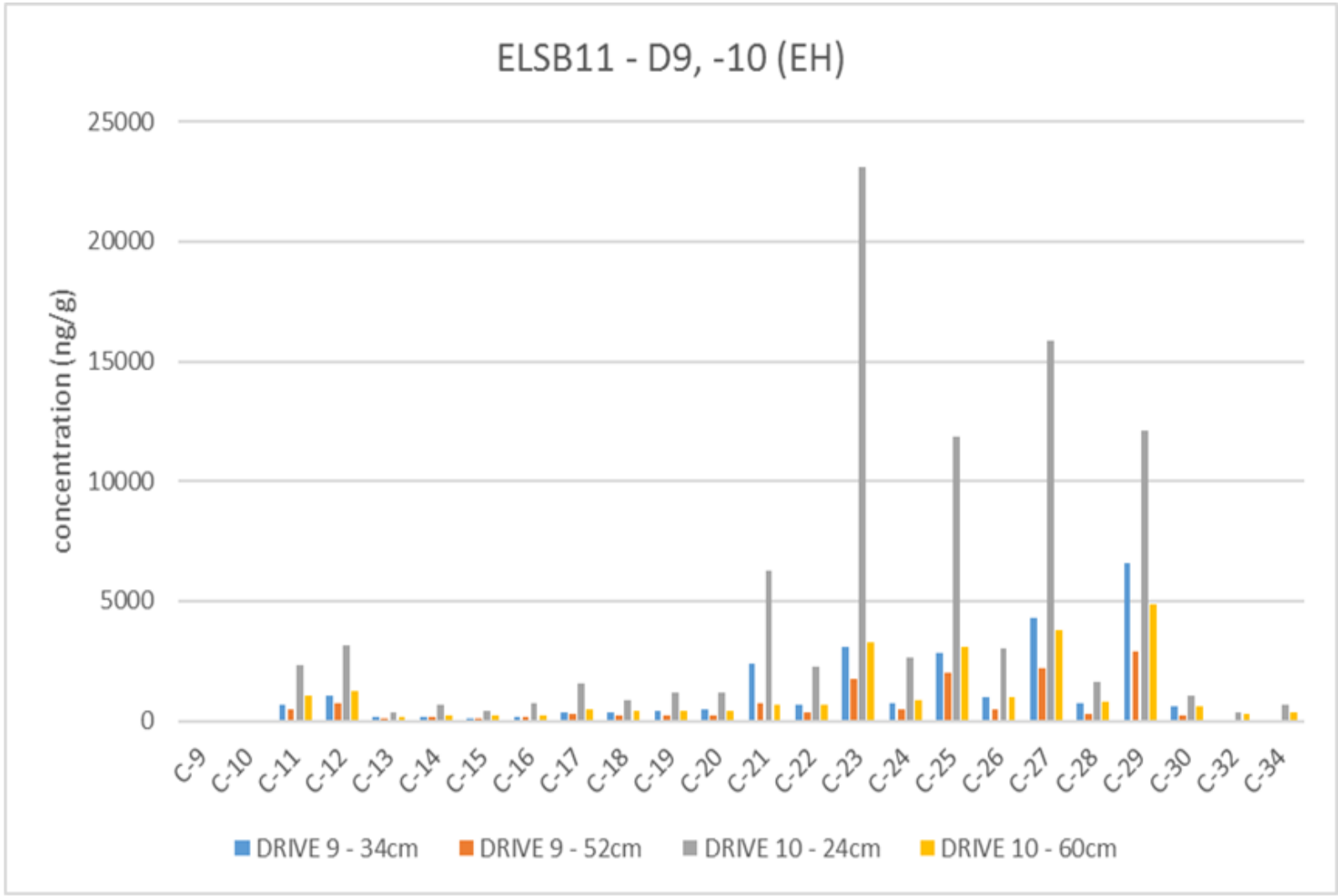
ELSB11 - D9, -10 (EH)
concentration (ng/g)
25000
20000
15000
10000
5000
0
C-9
C-10
C-11
C-12
C-13
C-14
C-15
C-16
C-17
C-18
C-19
C-20
C-21
C-22
C-23
C-24
C-25
C-26
C-27
C-28
C-29
C-30
C-32
C-34
DRIVE 9 - 34cm
DRIVE 9 - 52cm
DRIVE 10 - 24cm
DRIVE 10 - 60cm

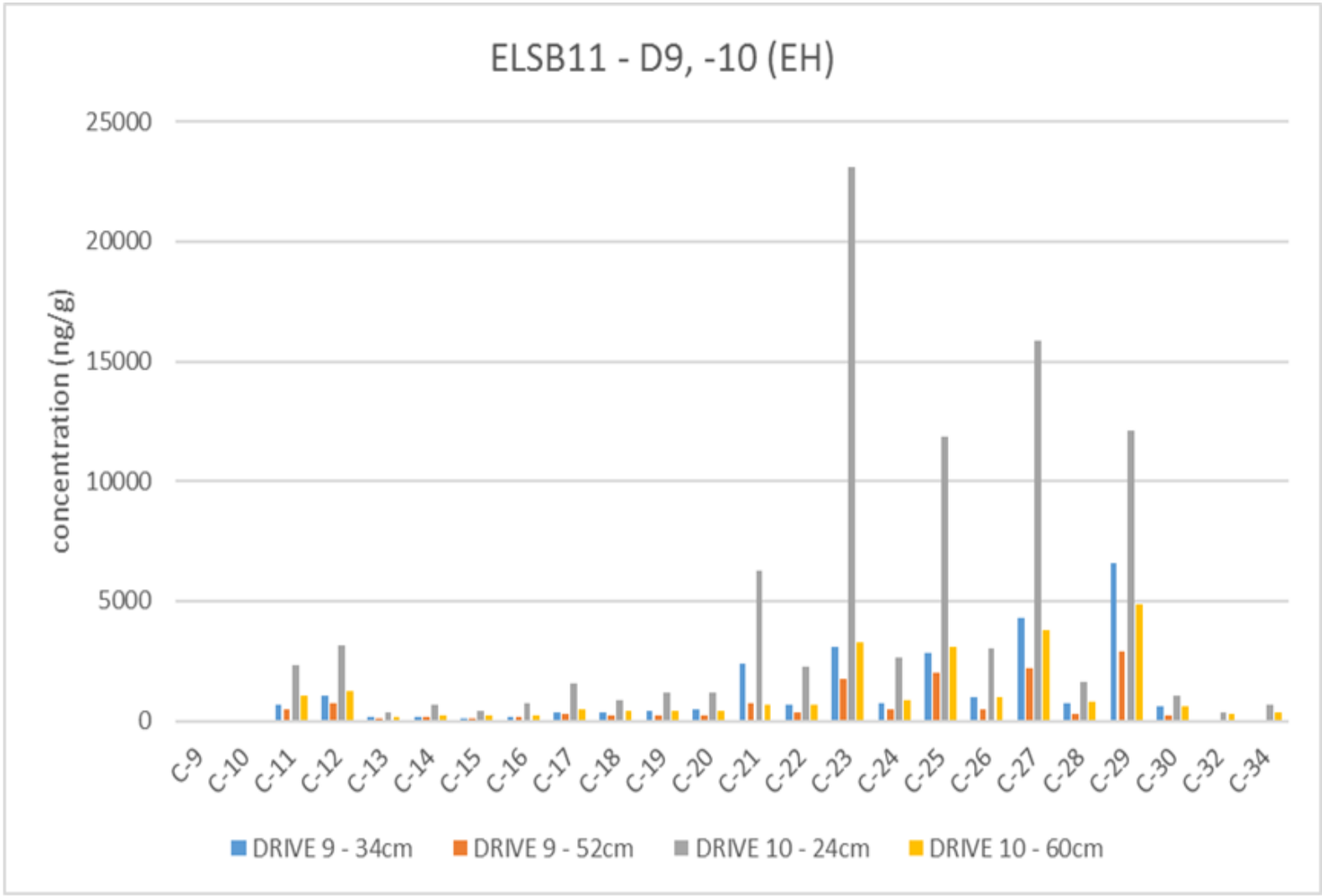
ELSB11 - D9, -10 (EH)
concentration (ng/g)
25000
20000
15000
10000
5000
0
C-9
C-10
C-11
C-12
C-13
C-14
C-15
C-16
C-17
C-18
C-19
C-20
C-21
C-22
C-23
C-24
C-25
C-26
C-27
C-28
C-29
C-30
C-32
C-34
DRIVE 9 - 34cm
DRIVE 9 - 52cm
DRIVE 10 - 24cm
DRIVE 10 - 60cm

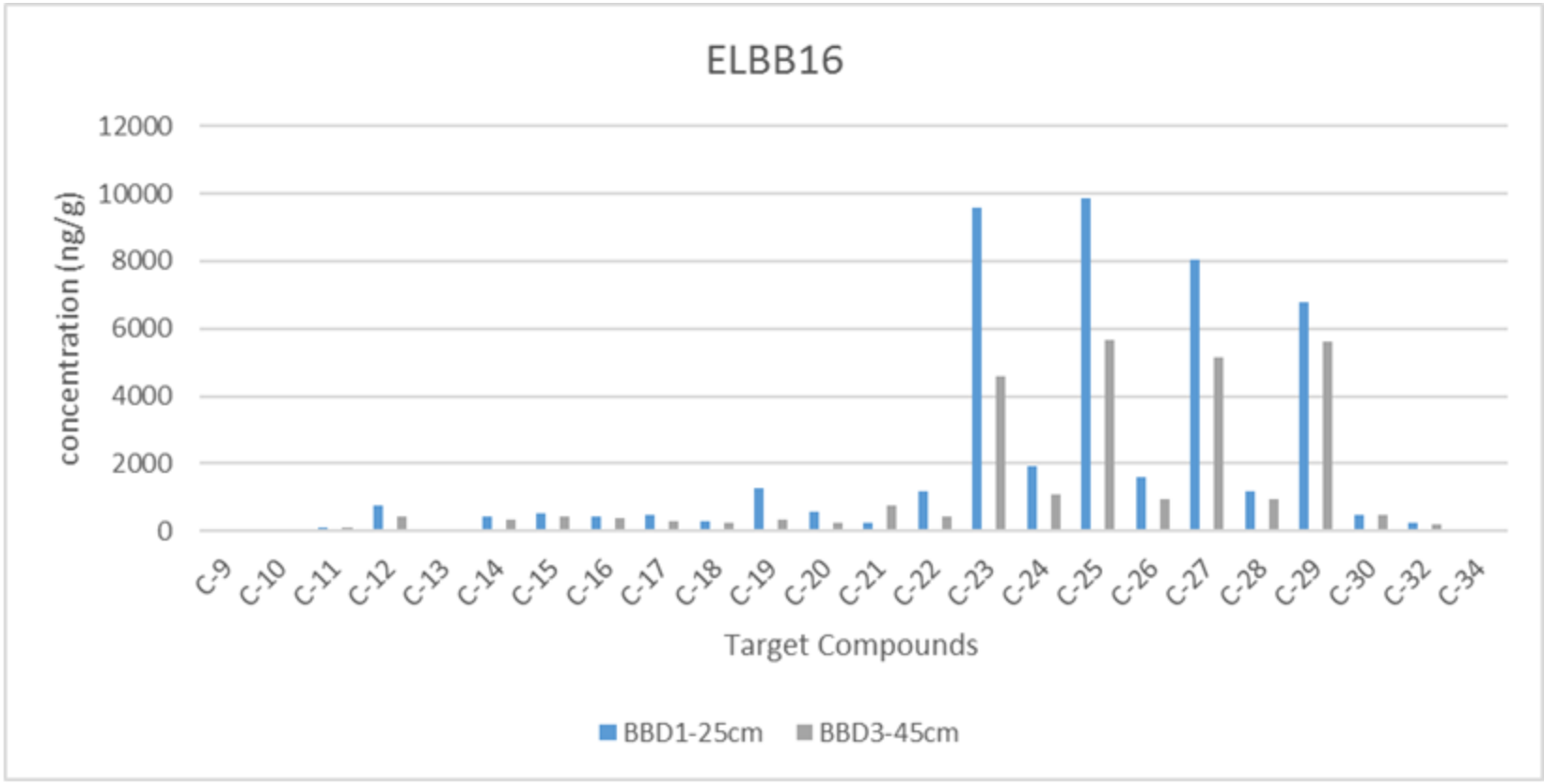
ELBB16
12000
10000
8000
6000
4000
2000
0
concentration (ng/g)
C-9
C-10
C-11
C-12
C-13
C-14
C-15
C-16
C-17
C-18
C-19
C-20
C-21
C-22
C-23
C-24
C-25
C-26
C-27
C-28
C-29
C-30
C-32
C-34
Target Compounds
BBD1-25cm
BBD3-45cm

ELSB-LATE HOLOCENE	0 cm	18 cm	76 cm	96 cm
C-9	0	0	0	371.99
C-10	0	0	0	659.26
C-11	2210.64	677.22	1582.84	2088.09
C-12	2791.18	1379.99	2431.87	3052.88
C-13	350.72	197.1	309.42	442.01
C-14	354.69	301.07	394.03	701.4
C-15	379.89	179.72	325.37	569.26
C-16	565.04	459.98	463.27	762.09
C-17	1363.35	801.9	893.37	1595.95
C-18	1083.01	686.41	977.83	1770.93
C-19	4096.16	1245.97	1839.91	3540.44
C-20	1412.67	853.99	909.53	1952.69
C-21	3163	2403.83	4025.6	4672.92
C-22	1624.32	1644.97	2191.39	2555.02
C-23	10596.86	10210.02	14528.53	21849.69
C-24	2136.43	1918.85	2821.04	3382.21
C-25	9853.22	7855.08	8746.51	9850.35
C-26	2045.33	1503.4	2198.95	2282.83
C-27	7111.59	6158.46	7066.98	9850.35
C-28	1434.74	1274.85	2516.41	2710.48
C-29	13068.59	7387.55	12312.19	7552.83
C-30	877.8	629.54	1075.71	1535.44
C-32	455.17	264.39	357.84	429.24
C-34	0	0	0	0

ELSB-EARLY HOLOCENE	478 cm	496 cm	560 cm	595 cm
C-9	0	0	0	0
C-10	0	0	0	0
C-11	652.88	476.03	2315.5	1057.93
C-12	1054.4	725.43	3142.59	1245.78
C-13	167.92	84.42	339.15	178.5
C-14	173.74	165.31	685.92	235.25
C-15	114.42	90.11	436.36	194.57
C-16	158.93	178.77	753.58	224.41
C-17	372.48	306.36	1559.86	453.18
C-18	367.17	207.78	888.97	393.53
C-19	411.55	211.89	1146.74	411.63
C-20	447.37	228.67	1153.23	388.86
C-21	2382.8	734.4	6284.96	687.26
C-22	696.84	348.46	2252.69	647.11
C-23	3116.74	1773.85	23123.1	3272.65
C-24	705.67	452.29	2668.08	829.95
C-25	2799.93	1985.68	11852.9	3090.92
C-26	961.65	455.96	3048.7	989.96
C-27	4283.69	2219.62	15868	3803.37
C-28	719.75	289.23	1611.94	805.09
C-29	6586.54	2875.92	12089.8	4890.91
C-30	574.37	246.42	1052.14	613.03
C-32	0	0	346.62	291.4
C-34	0	0	649.45	379.55

ELBB16	25 cm	84 cm
C-9	0	0
C-10	0	0
C-11	120.3	98.13
C-12	734.55	451.29
C-13	65.97	50.44
C-14	413.04	343.05
C-15	509.28	448.78
C-16	447.44	389.99
C-17	477.5	301.23
C-18	305.41	224.87
C-19	1248.36	329.54
C-20	586.29	237.56
C-21	258.43	738.47
C-22	1180.96	449.98
C-23	9562.13	4591.55
C-24	1932.27	1098.06
C-25	9872.37	5675.26
C-26	1609.75	943.76
C-27	8035.77	5140.17
C-28	1179.39	947.8
C-29	6793.29	5614.99
C-30	495.04	452.09
C-32	227.59	199.396
C-34		0

APPENDIX D

BIOGENIC SILICA DATA

ELSB11-LATE HOLOCENE SECTION	True Depth (cm)	wt % Bsi
	8	4.464933
	16	3.845333
	36	4.102
	76	5.0736
	96	2.892
	108	5.6636
	116	3.541067
	128	4.161067
	136	5.6104

ELSB11-EARLY HOLOCENE SECTION	True Depth (cm)	wt % Bsi
	303	6.995467
	317	5.681467
	333	7.706
	341	8.920667
	349	8.367733
	380	7.412267
	392	9.568133
	400	9.042
	420	5.094
	432	7.684133
	454	11.44973
	462	11.9604
	476	12.52227
	488	12.44293
	545	9.404667
	555	11.33293
	565	8.146267
	585	10.78427
	595	10.29467

ELBB-16	Depth(cm)	concentration	Bsi (%)
	8	33.487	4.464933
	18	28.84	3.845333
	36	30.765	4.102
	42	32.874	4.3832
	75	38.052	5.0736
	95	21.69	2.892
	110	42.477	5.6636
	115	26.558	3.541067
	130	31.208	4.161067
	140	42.078	5.6104
	145	33.217	4.428933
	160	31.57	4.209333
	170	27.798	3.7064

REFERENCES

REFERENCES

Anderson, L., 2011, Holocene record of precipitation seasonality from lake calcite $\delta^{18}O$ in the Central Rocky Mountains, United States: Geology, v. 39, p. 211-214.

Anderson, L., Berkelhammer, M., Barron, J.A., Steinman, B.A., Finney, B.P., and Abbott, M.B., 2016, Late oxygen isotopes as recorders of North American Rocky Mountain hydroclimate: Holocene patterns and variability at multi-decadal to millennial time scales: Global and Planetary Change, v. 137, p. 131-148.

Bacon, C. R., 1983, Eruptive history of Mount Mazama and Crater Lake caldera, Cascade Range, USA: Journal of Volcanology and Geothermal Research, v. 18, p. 57-115.

Baker, P., Seltzer, G., Fritz, S., Dunbar, R.B., Grove, M.J., Tapia, P.M., Cross, S.L., Rowe, H.D., and Broda, J.P., 2001, The history of South American tropical precipitation for the past 25,000 years: Science, v. 291, p. 640-643.

Barron, J. A., and Anderson, L., 2011, Enhanced late Holocene ENSO/PDO expression along the margins of the eastern North Pacific: Quaternary International, v. 235, p.3-12.

Barron, J.A., Metcalfe, S.E., and Addison, J.A., 2012, Response of the north American monsoon to regional changes in ocean surface temperature: Paleoceanography, v. 27, 17 p.

Basara, J.B., Maybourn, J.N., Peirano, C.M., Tate, J.E., Brown, P.J., Hoey, J.D., and Smith, B.R., 2013, Drought and associated impacts in the Great Plains of the United States: A review: International Journal of Geosciences, v. 4, p. 72-81.

Bateson, O., 2016, Everything you ever wanted to know about the Bly Tunnel: www.susanvillestuff.com (accessed January 2016).

Benson, L.V., and White, J.W.C., 1994, Stable isotopes of oxygen and hydrogen in the Truckee River Pyramid Lake surface water system 3: Source of water vapor overlying Pyramid Lake: Limnology Oceanography, v. 39, p. 1945-1958.

Benson, L.V., Kashgarian M., Rye, R.O., Lund, S.P., Paillet, F.L., Smoot, J., Kester, C., Mensing, S., Meko, D., and Lindstrom, S., 2002, Holocene multidecadal and multicentennial droughts affecting northern California and Nevada: Quaternary Science Reviews, v. 21, p. 659-682.

Bird, B.W., and Kirby, M.E., 2006, An alpine lacustrine record of early Holocene North American monsoon dynamics from Dry Lake, southern California (USA): Journal of Paleolimnology, v. 35, p. 179-192.

Briles, C.E., Whitlock, C., and Bartlein, P.J., 2005, Postglacial vegetation, fire and climate history of the Siskiyou Mountains, Oregon, USA: Quaternary Research, v. 64, p. 44-56.

Briles, C.E., Whitlock, C., Skinner, C.N., and Mohr, J., 2011, Holocene forest development and maintenance on different substrates in the Klamath Mountains, northern California, USA: Ecology, v. 92, no. 3, p. 590-601.

Cahoon, D. J., 1974, Eagle Lake Limnological Data and Nutrient Study: Susanville, CA, The Resource Agency, California Department of Water Resources, Northern District. 122 p.

Caporaletti, M., 2011, Ostracods and stable isotopes: Proxies for paleoenvironmental reconstructions: Joannea Geologie und Paläontologie, v. 11, p. 345-359.

Cayan, D.R., Redmond, K.T., and Riddle, L.G., 1999, ENSO and hydrologic extremes in the western United States: American Meteorological Society, v. 12, p. 2881-2893.

Chatters, J. C., 1991, Paleoecology and paleoclimates of the Columbia Basin, Northwest America: Richland, Washington, Pacific Northwest Laboratory, PNLSA-18715.

Chivas, A.R., De Deckker, P., and Shelley, J.M.G., 1986, Magnesium and strontium in non-marine ostracod shells as indicators of palaeosalinity and palaeotemperature: Hydrobiologia, v. 143, p. 135-142.

Choi, J., Lu, J., Son, S., Frierson, D.M.W., and Yoon, J., 2016, Uncertainty in future projections of the North Pacific subtropical high and its implication for California winter precipitation change: Journal of Geophysical Research, v. 121, no. 2, p. 795-806.

Clynne, M.A., 1999, A complex magma mixing origin for rocks erupted in 1915, Lassen Peak, California: Journal of Petrology, v. 40, no. 1, p. 105-132.

COHMAP Members, 1988, Climatic changes of the last 18,000 years: Observations and model simulations: Science, v. 241, no. 4869, p. 1043-1052.

Cook, B.I., Ault, T.R., and Smerdon, J.E., 2015, Unprecedented 21st century drought risk in the American Southwest and Central Plains: Science Advances, v. 1, 7 p.

Cook, E. R., Seager, R., Cane, M.A., and Stahl, D.W., 2007, North American drought: reconstructions, causes, and consequences: Earth Science Review, v. 81, no.1-21, p. 93-134.

Conley, D.J., and Schelske, C.L., 2001, Biogenic silica, *in* Smol, J.P., Birks, H.J.B., Last, W.M., eds., Tracking environmental change using lake sediments: Berlin, SpringerLink, Developments in Paleoenvironmental Research 3, p. 281-293.

Cowart, A., and Byrne, R., 2013, A paleolimnological record of late Holocene vegetation change from the central California Coast: California Archaeology, v. 5, no. 2, p. 337-352.

Davis, L.G., and Muehlenbachs, K., 2001, A late Pleistocene to Holocene record of precipitation reflected in margaritifera falcata shell $\delta^{18}O$ from three archaeological sites in the lower Salmon River Canyon, Idaho: Journal of Archeology Science, v. 28, p. 291-303.

Dean, W.E., 1974, Determination of carbonate and organic matter in calcareous sedimentary rocks by loss on ignition: Comparison with other methods: Journal of Sedimentary Petrology, v. 44, p. 242-248.

Dettinger, M.D., Cayan, D.R., Diaz, H.F., and Meko, D.M., 1998, North-South precipitation patterns in western North America on interannual-to-decadal timescales: Journal of Climate, v. 11, p. 3095-3111.

Dingemans, T., Mensing, S.A., Feakins, S.J., Kirby, M.E., and Zimmerman, S.R.H., 2014, 3000 years of environmental change at Zaca Lake, California, USA: Frontiers in Ecology and Evolution, v. 2, no. 34, 16 p.

Eglinton, G., and Logan, G.A., 1991, Molecular Preservation: Philosophical Transactions of the Royal Society B: Biological Sciences v. 333, p. 315-328.

Eglinton, G., and Hamilton, R.J., 1963, The distribution of alkanes, *in* Swain, T., ed., Chemical Plant Taxonomy: London, UK, Academic Press, p. 187-217.

El Frihmat, Y., Hebbeln, D., Jaaidi, E. B., and Mhammdi, N., 2015, Reconstruction of productivity signal and deep-water conditions in Moroccan Atlantic margin (~35°N) from the last glacial to the Holocene: SpringerPlus, v. 4, no. 69, http://doi.org/10.1186/s40064-015-0853-6.

Enzel, Y., Brown, W.J., Anderson, R.Y., McFadden, L.D., and Wells, S.G., 1992, Short-duration Holocene lakes in the Mojave River drainage basin, southern California: Quaternary Research, v. 38, p. 60-73.

Felmy, A., and Weare, J.H., 1986, The prediction of borate mineral equilibria in natural waters: Application to Searles Lake, CA: Geochimica et Cosmochimica Acta, v. 50, p. 2771-2783.

Ficken, K.J., Li, B., Swain, D.L., and Eglinton, G., 2000, An n-alkane proxy for the sedimentary input of submerged/floating freshwater aquatic macrophytes: Organic Geochemisty, v. 31, no. 7-8, p. 745-749.

Galloway, J.N., and Cowling, E.B., 1978, The effects of precipiation on aquatic and terrestrial ecosystems: A proposed precipitation chemistry network: Journal of the Air Pollution Control Association, v. 28, no. 3, p. 229-235.

Gester, G.C., 1962, The geological history of Eagle Lake, Lassen County, California: Occasional Papers of the California Academy of Sciences, no. 34, p. 1-24.

Grigg, L. D., and Whitlock, C., 1998, Late-glacial vegetation and climate changes in western Oregon: Quaternary Research, v. 49, p. 287-298.

Grose, T.L.T., Saucedo, G.J., and Wagner, D.L., 1992, Geologic map of the Eagle Lake quadrangle, Lassen County, California: California Department of Conservation Division of Mines and Geology Open-File Report 92-14, scale 1:100,000.

Holmes, J.A., 1996, Trace-element and stable isotope geochemistry of non-marine ostracod shells in Quaternary palaeoenvironmental reconstruction: Journal of Paleolimnology, v. 15 p. 223-235.

Holmgren, C.A., Betancourt, J.L., and Rylander, K.A., 2009, A long-term vegetation history of the Mojave-Colorado desert ecotone at Joshua Tree National Park: Journal of Quaternary Science, 15 p., doi: 10.1002/jqs.1313.

Johnson, T., Brown, E., McManus, J., Barker, P., and Gasse, F., 2002, A high-resolution paleoclimate record spanning the past 25,000 years in southern East Africa: Science, v. 296, p. 113-114.

Kaufmann, W., 1900, Elektrodynamische eigentumlichkeiten leitender gase: Annual Physiology, v. 307, p. 158-178.

Kirby, M.E., Lund, S.P., Anderson, M.A., and Bird, B.W., 2007, Insolation forcing of Holocene climate change in Southern California: A sediment study from Lake Elsinore: Journal of Paleolimnology, v. 38, p. 395-417.

Kirby, M.E., Lund, S.P., Patterson, W.P., Anderson, M.A., Bird, B.W., Ivanovici, L., Monarrez, P., and Nielson, S., 2010, A Holocene record of pacific decadal oscillation (PDO)-related hydrologic variability in southern California (Lake Elsinore, CA): Journal of Paleolimnology, v. 44, p. 819-839.

Kirby, M.E., Poulsen, C.H., Lund, S.P., Patterson, W.P., Reidy, L, and Hammond, D.E., 2004, Late Holocene lake level dynamics inferred from magnetic susceptibility and stable oxygen isotope data: Lake Elsinore, southern California (USA): Journal of Paleolimnology, v. 31, p. 275-293.

Kirby, M.E., Zimmerman, S.R.H., Patterson, W.P., and Rivera, J.J., 2012, A 9170-year record of decadal-to-multi-centennial scale pluvial episodes from the coastal southwest United States: A role for atmospheric rivers: Quaternary Science Reviews, v. 46, p. 57-65.

Kottek, M., Grieser, J., Beck, C., Rudolf, B., and Rubel, F., 2006, World map of the Koppen-Geiger climate classification updated: Meteorologische Zeitshchrift, v. 15, no. 3, p.259-263.

Kutzbach, J.E., 1981, Monsoon climate of the early Holocene: Climatic experiment using the earth orbital parameters for 9000 years ago: Science, v. 234, p. 59-61.

Langenbrunner, B., Neelin, D.J., Lintner, B.R., and Anderson, B.T., 2015, Patterns of precipitation change and climatological uncertainty among CMIP5 Models, with a focus on the midlatitude pacific storm track: Journal of Climate, v. 26, p. 4431-4446.

Li, H.C., and Ku, T.L., 1997, $\delta^{13}C$-$\delta^{18}O$ covariance as a paleohydrological indicator for closed-basin lakes: Palaeogeography, Palaeoclimatology, and Palaeoecology, v. 133, p. 69-80.

Mann, M.E., 2002, Little Ice Age, The earth system: Physical and chemical dimensions of global environmental change, v. 1, p. 504-509.

Mantua, N.J., and Hare, S.R., 2002, The pacific decadal oscillation: Journal of Oceanography, v. 58, p. 35-44.

Mantua, N.J., Hare, S.R., Zhang, Y., Wallace, J.M., and Francis, R.C., 1997, A pacific interdecadal climate oscillation with impacts on salmon production: Joint Institute for the Study of Atmosphere and Ocean, v. 78, no. 6, p. 1069-1079.

Maslin, P.E., and Boles, G.L., 1978, Use of multiple addition bioassay to deline limiting nutrients in Eagle Lake: Hydrobiologia, v. 58, p. 261-269.

Maurer, M.K., Menounos, B., Luckman, B.H, Osborn, G., Clague, J.J., Beedle, M.J., Smith, R., and Atkinson, N., 2012, Late Holocene glacier expansion in the Cariboo and northern Rocky Mountains, British Columbia, Canada: Quaternary Science Reviews, v. 51, p. 71-80.

Mauquoy, D., Van Geel, B., Blaauw, M. and Van Der Plicht, J., 2002, Evidence from northwest European bogs shows 'Little Ice Age' climatic changes driven by variations in solar activity: The Holocene, v. 12, p. 1-6.

McCabe, G.J., and Dettinger, M.D., 1999, Decadal variations in the strength of ENSO teleconnections with precipitation in the western United States: International Journal of Climatology, v. 19, p. 1399-1410.

McCabe, G.J., Palecki, M.A., and Betancourt, J.L., 2004, Pacific and Atlantic Ocean influences on multidecadal drought frequency in the United States: Proceedings of the National Academy of Sciences, v. 101, no. 12, p. 4136-4141.

McKee, T.B., Doesken, N.J., and Kleist, J., 1993, The relationship of drought frequency and duration to time scales, *in* Proceedings of the 8th conference on Applied Climatology: Boston, MA, American Meteorological Society, v. 17, no. 22, p. 179-183.

Mehringer, P.J., 1985, Late-Quaternary pollen records from the interior Pacific Northwest and northern Great Basin of the United States, *in* Bryant, V.M., Jr., and Holloway, R.G., eds., Pollen Records of Late-Quaternary North American Sediments: Dallas, Texas, American Association of Stratigraphic Palynologists, p. 167-187.

Mensing, S.A., 1998, 560 years of vegetation change in the region of Santa Barbara, California: Madroño, v. 45, 11 p.

Mensing, S.A., Benson, L., Kashgariank, M., and Lund, S., 2004, A Holocene pollen record of persistent droughts from Pyramid Lake, Nevada, USA: Quaternary Research, v. 62, p. 29-38.

Meyers, P.A., 1994, Preservation of elemental and isotopic source identification of sedimentary organic matter: Chemical Geology, v. 114, p. 289-302.

Meyers, P.A., 1997, Organic geochemical proxies of paleoceanographic, paleolimnologic, and paleoclimatic processes: Organic Geochemistry, v. 27, no. 5/6, p. 213-250.

Meyers, P.A., and Ishiwatari, R., 1993, Lacustrine organic geochemistry: An overview of indicators of organic matter sources and diagenesis in lake sediments: Organic Geochemistry, v. 20, no. 7, p. 867-900.

Meyers, P.A., and Lallier-Verges, E., 1998, Lacustrine sedimentary organic matter records of Late Quaternary Paleoclimates: Journal of Paleolimnology, v. 21, p. 345-372.

Moy, C.M., Seltzer, G.O., Rodbell, D.T., and Anderson, D.M., 2002, Variability of El Nino/Southern Oscillation activity at millennial timescales during the Holocene epoch: Nature, v. 420, p. 162-165.

Munsell Color, 2010, Munsell Soil-Color Charts: With genuine Munsell color chips: Grand Rapids, Michigan, Munsell Color.

Negrini, R.M., Erbes, D.B., Faber, K., Herrera, A.M., Roberts, A.P., Cohen, A.S., Wigand, P.E., and Foit, F.F., Jr., 2000, A paleoclimate record for the past 250,000 years from Summer Lake, Oregon, USA: I Chronology and magnetic proxies for lake level: Journal of Paleolimnology, v. 24, p. 125-149.

Negrini, R.M., Wigand, P.E., Draucker, S., Gobalet, K., Gardner, J.K., Sutton, M.Q., and Yohe, R.M., II, 2006, The rambla highstand shoreline and the Holocene lake-level history of Tulare Lake, California, USA: Quaternary Science Reviews, v. 25, p. 1599-2006.

Piechota, T.C., Dracup, J.A., and Fovell, R.G., 1997, Western US streamflow and atmospheric circulation patterns during El Nino-Southern Oscillation: Journal of Hydrology, v. 201, p. 249-271.

Prahl F.G., Bennett J.T., and Carpenter R., 1980, The early diagenesis of aliphatic hydrocarbons and organic matter in sedimentary particulates from Dabob Bay, Washington: Geochimica et Cosmochimica Acta, v. 44, p. 1967-1976.

Purdy, T. I., 1988, Purdy's Eagle Lake: Susanville, California, Lahonton Images.

Redmond, K.T., and Koch, R.W., 1991, Surface climate and streamflow variability in the western United States and their relationship to large scale circulation indices: Water Resources Research, v. 27, no. 9, p. 2381-2399.

Roberts, C.T., and Gross, T.L.T., 1982, Late Cenozoic extensional strain rates and directions in the Honey Lake-Eagle Lake region, northeast California: Earth and Space Science, Transactions American Geophysical Union, v. 63, p. 1107.

Ropelewski, C.F., and Halpert, M.S., 1987, Global and regional scale precipitation patterns associated with the El Niño/Southern Oscillation: Monthly Weather Review, v. 115, no. 8, p. 1606-1626.

Ropelewski, C.F., and Halpert, M.S., 1989, Precipitation patterns associated with the high index phase of the southern oscillation: Journal of Climate, v. 2, no. 3, p. 268-284.

Schelske, C.L., Conley, D.J., Stoermer, E.F., Newberry, T.L., and Campbell, C.D., 1986, Biogenic silica and phosphorus accumulation in sediments as indices of eutrophication in the Laurentian Great Lakes: Hydrobiologia, v. 143, p. 79-86.

Shuman, B.N., Bartlein, P.J., Logar, N., Newby, P., and Webb, T., 2002, Parallel climate and vegetation responses to the early Holocene collapse of the Laurentide ice sheet: Quaternary Science Reviews, v. 21, p. 1793-1805.

Steinman, B.A., Rosenmeier, M.F., and Abbott, M.B., 2010, The isotopic and hydrologic response of small, closed-basin lakes to climate forcing from predictive models: Simulations of stochastic and mean-state precipitation variations: Limnological Oceanography, v. 55, no. 6, p. 2246-2261.

Stuiver, M., and Reimer, P. J., 1993, Extended ^{14}C database and revised CALIB radiocarbon calibration program: Radiocarbon, v. 35, p. 215-230.

Swain, D.L., 2015, A tale of two California droughts: Lessons amidst record warmth and dryness in a region of complex physical and human geography: Geophysical Research Letter, v. 42, p. 9999-10003.

Swain, D.L., Horton, D.E., Singh, D., and Diffenbaugh, N.S., 2016, Trends in atmospheric patterns conducive to seasonal precipitation and temperature extremes in California: Science Advances, p. 1-13, doi: 2:e1501344.

Swain, D. L., Tsiang, M., Haugen, D., Singh, A., Charland, A., Rajaratnam, B., and Diffenbaugh, N.S., 2014, The extraordinary California drought of 2013/2014: Character, context, and the role of climate change: Bulletin of the American Meteorological Society, v. 95, no. 9, p. S3-S7.

Sweeney, R. E., and Kaplan, I.R., 1980, Natural abundances of 15N as a source indicator for near-shore marine sedimentary and dissolved nitrogen: Marine Chemistry, v. 9, p. 81-94.

Thompson, D.M., Ault, T.R., Evans, M.N., Cole, J.E., and Emile-Geay, J., 2011, Comparison of observed and simulated tropical climate trends using a forward model of coral $\delta^{18}O$: Geophysical Research Letter, v. 38, L14706, doi:10.1029/2011GL048224.

Wallace, J.M., and Quanrong, J., 1991, Atmospheric-ocean interaction and teleconnection in the northern Pacific during cold season: Acta Meterologica Sinica, v. 11, no. 4, p. 537-546.

White, I.R., and Crider, J.G., 2006, Extensional fault propagation folds: Mechanical models and observations from the Modoc Plateau, northeastern California: Journal of Structural Geology, v. 28, p. 1352-1370.

Whitlock, C., 1992, Vegetational and climatic history of the Pacific Northwest during the last 20,000 years: Implications for understanding present-day biodiversity: The Northwest Environmental Journal, v. 8, p. 5-28.

Whitlock, C., and Bartlein, P.J., 1993, Spatial variations of Holocene climatic change in the Yellowstone region: Quaternary Research, v. 39, p. 231-238.

Wise, E.K., 2010, Spatiotemporal variability of the precipitation dipole transition zone in the western United States: Geophysical Research Letters, v. 37, p. 1-5.

Wise, E.K., 2016, Five centuries of U.S. West Coast drought: Occurrence, spatial distribution, and associated atmospheric circulation patterns: Geophysical Research Letters, v. 43, no. 9, p. 4539-4546.

Wright, H.E., 1967, A square-rod piston sampler for lake sediments: Notes: Journal of Sedimentary Petrology, v. 37, no. 3, p. 975-976.

Wright, H.E., 1972, Quaternary history of Minnesota, *in* Sims, P.K., and Morey, G.B., eds., Geology of Minnesota: A Centennial Volume: Duluth, Minnesota, Minnesota Geological Survey, p. 515-578.

Zhang, Y., Wallace, J.M., and Battisti, D.S., 1996, ENSO-like interdecadal variability: 1900-1993: Journal of Climate, v. 10, p. 1004-1020.

Zheng, Y., Zhou, W., Meyers, P.A., and Xie, S., 2007, Lipid biomarkers in the Zoige-Hongyuan peat deposit: Indicators of Holocene climate changes in west China: Organic Geochemistry, v. 38, p. 1927-1940.